




Meteorites from the Lut Desert (Iran)

Hamed POURKHORSANDI ^{1,2*}, Jérôme GATTACCECA ¹, Pierre ROCHETTE ¹,
Massimo D'ORAZIO³, Hojat KAMALI⁴, Roberto de AVILLEZ⁵, Sonia LETICHEVSKY⁵,
Morteza DJAMALI⁶, Hassan MIRNEJAD⁷, Vinciane DEBAILLE², and A. J. Timothy JULI⁸

¹Aix Marseille Université, CNRS, IRD, Coll France, INRA, CEREGE, Aix-en-Provence, France

²Laboratoire G-Time, Université Libre de Bruxelles, CP 160/02, 50, Av. F.D. Roosevelt, 1050 Brussels, Belgium

³Dipartimento di Scienze della Terra, Università di Pisa, Via S. Maria 53, I-56126 Pisa, Italy

⁴Afshin Meteorite Hunting Group, Kerman, Iran

⁵Departamento de Engenharia Química e de Materiais, DEQM/PUC-Rio, Rua Marquês de São Vicente, 225, 22453-900 Rio de Janeiro, Brazil

⁶CNRS, Aix-Marseille Univ, Avignon Univ., IMBE, Aix-en-Provence, France

⁷School of Geology, College of Science, University of Tehran, Tehran 14155-64155, Iran

⁸Arizona AMS Laboratory, University of Arizona, Tucson, Arizona 85721, USA

*Corresponding author. E-mail: hamed.pourkhorsandi@ulb.ac.be

(Received 12 July 2018; revision accepted 29 April 2019)

Abstract—We present for the first time a detailed report on the discovery of a new meteorite collection region in the Lut Desert, eastern–southeastern Iran, describing its geological, morphological, and climatic setting. Our search campaigns, alongside with the activity of meteorite hunters, yielded >200 meteorite finds. Here, we report on their classification, spatial distribution, and terrestrial weathering. All the collected meteorites are ordinary chondrites (OCs). The most abundant by far are the highly weathered paired H5 distributed in the northwest of Kalut area (central Lut, Kerman dense collection area). The second are well-preserved paired L5 also found in Kalut region. A detailed study of the geochemistry and mineralogy of selected meteorites reveals significant effects of terrestrial weathering. Fe, Ni metal (hereafter simply metal) and troilite are transformed into Fe oxyhydroxides. A rather unusual type of troilite weathering to pyrite/marcasite is observed in most of the Lut Desert meteorites. Magnetic measurements and X-ray diffractometry confirm the occurrence of terrestrial weathering products, with the dominance of maghemite, goethite, and hematite. Mobile elements, such as Li, Sr, Mo, Ba, Tl, Th, and U, are enriched with respect to fresh falls. Meanwhile, a decrease in the V, Cr, Co, Rb (and possibly Fe) due to terrestrial weathering is detectable. The total carbon and CaCO₃ is higher than in samples from other hot deserts. The weathering effects observed in the Lut Desert OCs can be used as distinctive indicators to distinguish them from meteorites from other regions of the Earth. Measurements of terrestrial age (¹⁴C) show a range of 10–30 ka, which is in the range of ages reported for meteorites from other hot deserts except the Atacama Desert (Chile). Considering the high potential of the Lut Desert in meteorite preservation, systematic works should lead to the discovery of more samples giving access to interesting material for future studies.

INTRODUCTION

Besides Antarctica (Harvey 2003), hot deserts are suitable places for the preservation, the accumulation, and the subsequent recovery of meteorites. High

numbers of meteorites have been collected and studied from arid regions such as Atacama (Muñoz et al. 2007; Gattacceca et al. 2011; Hutzler et al. 2016), Sahara (Bischoff and Geiger 1995; Schlüter et al. 2002; Ouazaa et al. 2009), Australian deserts (Bevan and Binns 1989;

Bevan 1992; Benedix et al. 1999), Arabian Peninsula (Al-Kathiri et al. 2005; Gnos et al. 2009; Hezel et al. 2011; Hofmann et al. 2018), central (Rubin and Read 1984; Merriam and Harbaugh 2007) and southwestern United States (Zolensky et al. 1990; Rubin et al. 2000; Kring et al. 2001; Hutson et al. 2013), and Xinjiang Province in China (Li et al. 2017; Zeng et al. 2018). Finding new meteorite dense collection areas (DCAs) is important for (1) discovering new types of meteorites (e.g., Bischoff 2001; Kent et al. 2017; Pourkhorsandi et al. 2017a), (2) providing more samples for statistical works on the meteorite flux (e.g., Bland et al. 1996), (3) studying meteorite fall process by mapping strewnfields resulting from meteorite showers (e.g., Kring et al. 2001; Gnos et al. 2009), and (4) studying the alteration of extraterrestrial material in the terrestrial environment (Bland et al. 2006; Saunier et al. 2010; Uehara et al. 2012; Zurfluh et al. 2016; Pourkhorsandi et al. 2017b) also in relation with paleoclimate (Bland et al. 1998; Lee and Bland 2003; Pourkhorsandi et al. 2017b).

Iran is located in southwestern Asia, in the midlatitude belt of arid and semiarid regions of the Earth. Arid and semiarid areas cover more than 60% of the country. Despite its vast surface area ($1.75 \times 10^6 \text{ km}^2$) and dry climate, few meteorites were recorded until recently in Iran. Only two meteorites, both falls, were cataloged in the Meteoritical Bulletin during the 20th century: Veramin, a mesosiderite fallen in 1880 (Ward 1901; Graham and Hassanzadeh 1990) and Naragh, a H6 chondrite fallen in 1974 (Clarke 1975; Adib and Liou 1979). Shahdad, the first Iranian meteorite find, was collected in 2005 from the western margin of the Lut Desert (Garvie 2012). The Lut Desert, also known as Dasht-e-Lut, is located in the east-southeast of the country (Fig. 1a). Considering its climatic, geological, and geomorphological characteristics, Pourkhorsandi and Mirnejad (2013) proposed it as a potentially suitable place for meteorite preservation and collection.

The first systematic studies on meteorites from Iran and especially from the Lut Desert, were initiated in 2014 as a cooperation between CEREGE (Aix-en-Provence, France) and the University of Tehran (Iran). The start of the project was concurrent with local media coverage on meteorites by the first author, which raised interest of the Iranian public on this topic and promoted the formation of meteorite hunting groups. These groups are now active in different regions of the country, especially in the Lut region.

At the present time, less than 5 years after the beginning of the project, hundreds of meteorites have been collected from the Lut Desert and over 200 of these meteorites have been classified and approved by the Nomenclature Committee of the Meteoritical

Society. More samples are under classification. Besides our work, other groups have classified and studied meteorites from the Lut Desert (Hutson et al. 2014; Moggi-Cecchi et al. 2017; Pastukhovich et al. 2017; Ferrari et al. 2018). Most Lut Desert meteorites were collected in two DCAs from central Lut (CL) Desert: Lut and Kerman. The latter one encompasses most of the Kalut geographic region to the west (Fig. 1b), while the former covers the eastern Lut Desert, consisting in vast dune fields, a central gravel plain and a small part of the Kalut formation. From Gandom Beryan and Lut-e-Zangi Ahmad DCAs in the north and south (respectively) of Kerman and Lut DCAs, only 14 meteorites have so far been recovered.

In this work, we evaluate the potential of Lut Desert in Iran for meteorite recovery. We present data on the classification, weathering, and spatial distribution of 218 meteorites from the Lut Desert studied during this work. In addition, we report detailed geochemical and mineralogical characteristics of nine selected meteorites to investigate their weathering in this environment. Meteorites from different regions of the Lut Desert and from different ordinary chondrite (OC) groups are included. We also estimated the terrestrial age of three highly weathered meteorites from different regions of the desert to have a preliminary idea of the duration of meteorite accumulation in the Lut Desert.

ENVIRONMENT OF THE LUT DESERT

Geology and Geomorphology

The Lut Desert is a part of the Lut block which itself is a part of the Central Iranian microcontinent (Stocklin 1968). The Lut block is bounded to the north by Doruneh, to the east by Nehbandam, and to the west by Nayband fault systems. The South Jazmourian Fault confines the southern part of this block. More details on the geodynamical aspects of Iran and the region are given in Aghanabati (2004).

Based on geographic characteristics, Lut is divided into three main units (e.g., Dresch 1968). (1) Northern Lut is characterized by Cenozoic volcanic and sedimentary rocks and vast flat surfaces. (2) CL consists of three different parts (a) Kalut, which is megayardangs occupying the western part of CL (Figs. 1 and S1 in supporting information) (Mashhadi et al. 2002; Ehsani and Quiel 2008; Ghodsi 2017). These are among the largest desert forms of their kind on the planet. Long hills with height around 10 m (and 50 m in some cases) made of clays, silt, and sand, and also containing evaporites and carbonates, separated by large wind-swept parallel

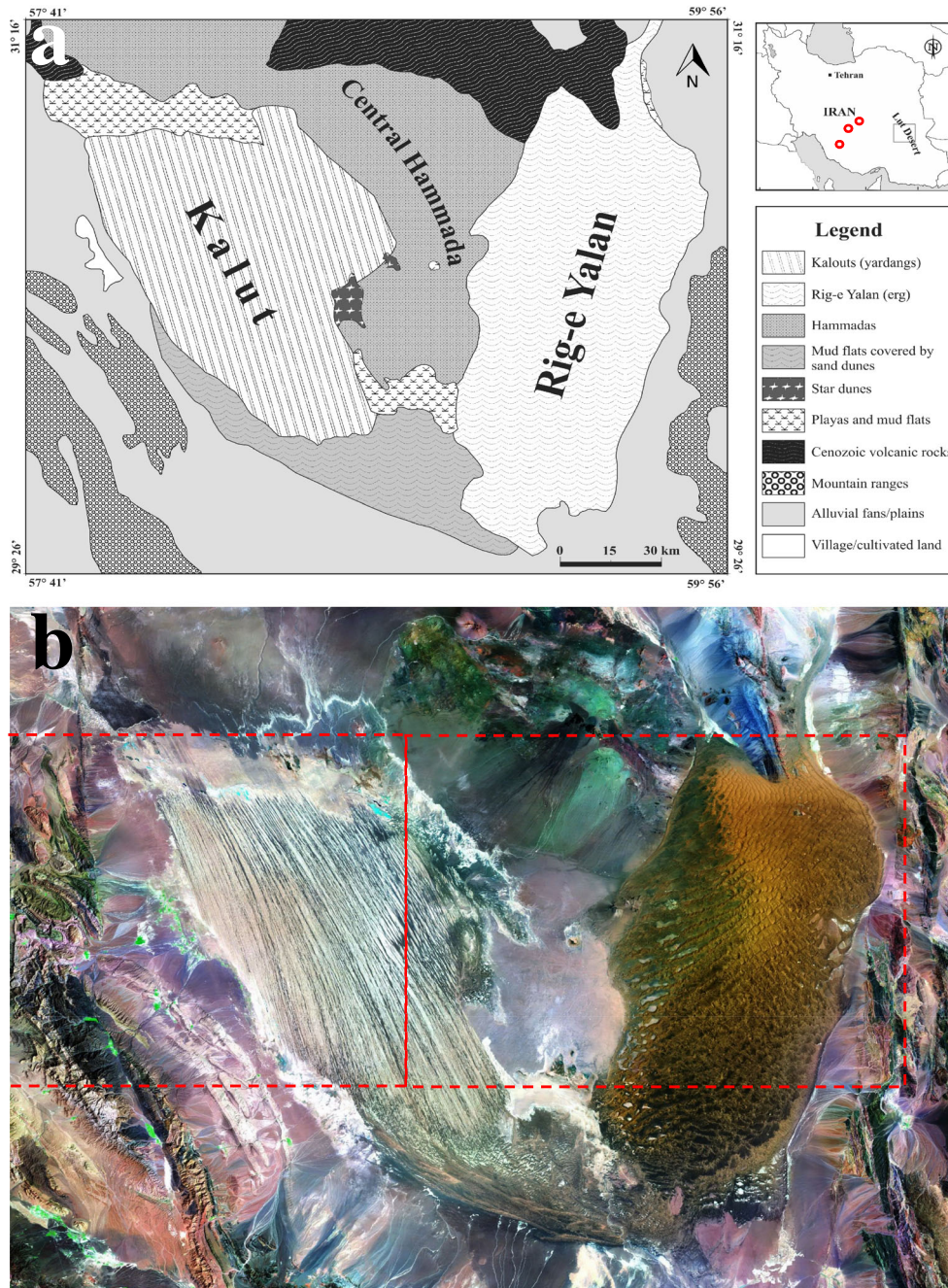


Fig. 1. a) Map of the central Lut Desert; adapted from Pourkhorsandi et al. (2017b). Circles on the Iran map show the location of Yazd, Abarkouh, and Sarvestan meteorites, respectively, from north to south. b) Landsat 8 satellite image of the central Lut Desert and the surrounding areas. Dashed quadrangles show the position of Kerman (west) and Lut (east) DCAs. (Color figure can be viewed at wileyonlinelibrary.com.)

corridors with a northwest–southeast direction extending over a 140×80 km area (Fig. S2 in supporting information); (b) Rig-e Yalan (Yalan Erg), the eastern unit of CL, is a sand sea comprising a great mass of dunes and sand rises with heights up to 475 m that cover an area of $\sim 50 \times 100$ km. (c) Playas, hammadas, and sand sheet type plains form

the middle part of CL. (3) Southern Lut is characterized by playas and ravines.

The accessibility through the Shahdad-Nehbandan road, and more importantly, the fine-grained nature of the local sediments, has made the Kalut the main target for meteorite hunting. Indeed, aside from its northern part, which is composed of highly saline Rude-e Shur

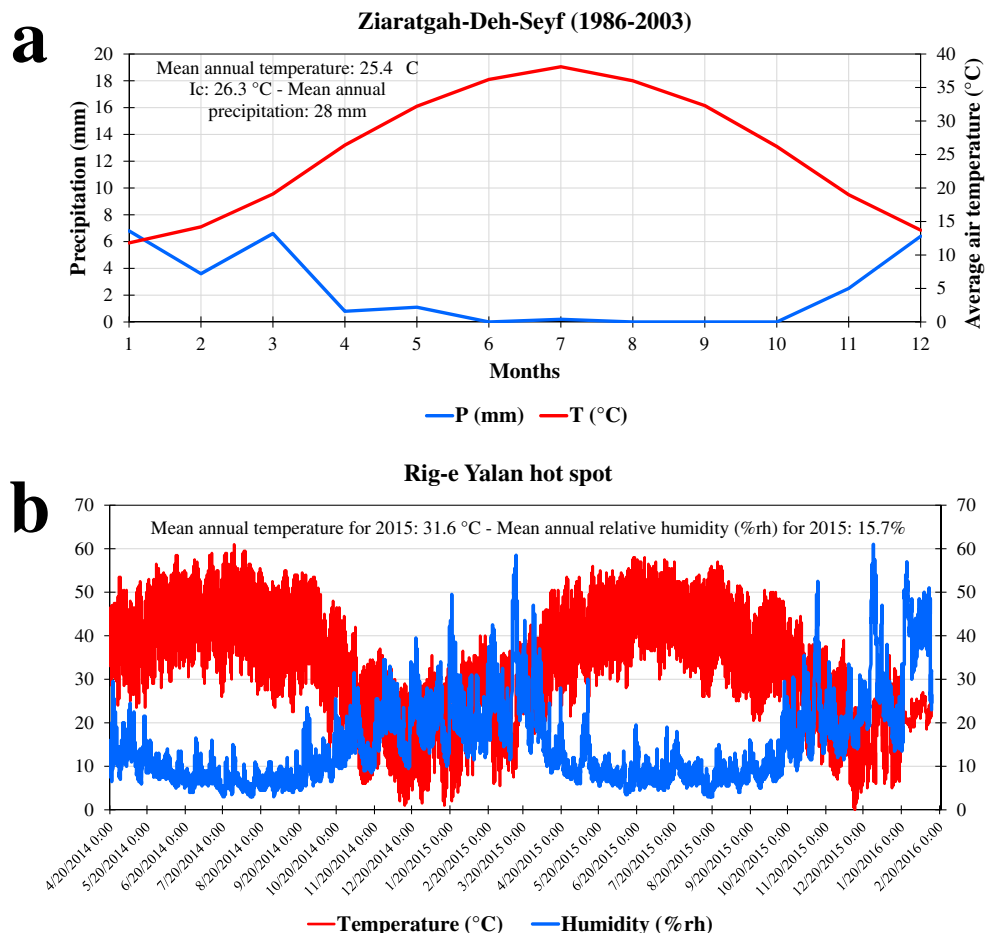


Fig. 2. a) Climate diagram of Ziaratgah-Deh-Seyf weather station near Shahdad. Note that according to index the dry season ($P < 2T$) lasts for 12 months. Data from Iran Meteorological Organization. b) One and half a year record of near ground surface variations in temperature and relative humidity. Data collected using a Lascar EL-USB-2 data logger with 1-hour interval records. (Color figure can be viewed at wileyonlinelibrary.com.)

river and the related clay-evaporite-rich puffy soils, the rest of the Kalut is dry and filled with fine-grained sand.

We analyzed three samples from top soil (1–10 cm) of the Kalut. The trace elemental composition of these samples is reported in Table S1 in supporting information. The majority of the elements are depleted in comparison to the mean upper continental crust (UCC) composition. Strontium in two soil samples from the Kalut (KS1 and KS3) shows a positive anomaly ($\times 2$), and a small negative anomaly in KS2. This might be the result of variable amount of carbonate content in soil. In general, Kalut soil samples show a homogeneous chemical composition. Regardless of these small-scale differences, a comparison of the Kalut soils and UCC chemical composition with that of mean CI chondrites shows very similar geochemical behavior between the soils and UCC without any significant difference.

Climate

High temperature, precipitation rate below 50 mm yr^{-1} , and high potential evaporation rate (5000 mm yr^{-1}) are the main climatic characteristics of the Lut Desert (Fig. 2a). The de Martonne aridity index (a classic indicator of dryness), which uses temperature and rainfall data, for CL is less than 1 and is 2–4 for the margins of the desert (e.g., Motamed 1974). Data from *Aqua*/MODIS Climate Model Grid shows that Rig-e Yalan of Lut Desert was the hottest region on the Earth in the years 2004, 2005, 2006, 2007, and 2009 with maximum surface temperatures of 68.0, 70.7, 68.5, 69.0, and 68.6 °C, respectively (Mildrexler et al. 2006, 2011). The Lut Desert is the only area in Iran with a Tropical Hyperdesertic climate, the driest possible bioclimate in the Global Bioclimatic Classification System (Djamali et al. 2011).

In order to obtain the first “long-term” in situ climatic data, we placed an automatic thermometer/hygrometer (Lascar EL-USB-2) in Rig-e Yalan and in the location shown to be the hottest spot (29°57.5'N, 59°4.3'E, 285 m) (Mildrexler et al. 2006). The instrument was placed inside a wooden box 20–30 cm above the ground and collected precise data with an interval record time of 60 min from April 2014 to February 2016. Temperature ranged from near 0 to 61 °C and relative humidity (rh) ranged from 3% to 61%. Mean annual air temperature and humidity for 2015 are 31.6 °C and 15.7% rh, respectively. Figure 2b shows the daily temperature and %rh variations. Note that high values of relative humidity are sometimes associated with high temperatures in winter months. For instance, during January 2016, the 30–50% rh occurred at 20–30 °C temperatures.

METHODOLOGY

Searching Methods

Meteorite searches have focused on the Kalut area in the Kerman DCA. Systematic searches were conducted both by car and foot. Low abundance of terrestrial rocks and the narrow valleys in the Kalut make searching by car easier and more efficient than by foot. In contrast to the Kalut, the presence of dark-colored surfaces covered by volcanic rocks in the interdunal areas of Rig-e Yalan and in the central hammada decreases the efficiency in finding meteorites. Although we have not done any systematic work in these areas, it seems that searching by foot is more fruitful (similar to e.g., the Atacama Desert). Low abundance of terrestrial rocks in the sheet sand plains of the Rig-e Yalan makes the search by car a better option.

Laboratory Methods

Macroscopic observations were done both on the exterior and cut surface of the meteorites. Polished thin and thick sections were prepared at CEREGE and a Leica DM2500P optical microscope was used for petrographic observations.

Magnetic susceptibilities were measured on whole samples using a KLY2 susceptibility meter from Agico equipped with a large coil (inner diameter of 8 cm) and a SM150 susceptibility meter from ZH instruments for smaller samples. Magnetic susceptibility is expressed as the decimal logarithm of χ in $10^{-9} \text{ m}^3 \text{ kg}^{-1}$ in order to account for the five orders of magnitude variation in rocks. For strongly magnetic material ($\log \chi > 3$), χ is proportional to the amount of metal, magnetite,

maghemite, cohenite, and schreibersite, i.e., minerals with practically equal specific χ . A combination of magnetic susceptibility data with microscopic observations is an effective way to classify OCs and evaluate pairing. After randomly checking the olivine and pyroxene chemistry for different samples with identical petrographic and magnetic properties and obtaining similar coherent results, we classified paired meteorites using only magnetic susceptibility data and petrographic observations, and taking into account their geographic distribution. Magnetic susceptibility can be used as a pairing tool because the variation in magnetic susceptibility within a meteorite is smaller than the intermeteorite variation in a given group (Rochette et al. 2003; Folco et al. 2006; Gattacceca et al. 2014). Hysteresis properties for five selected meteorites were measured with a Princeton Micromag vibrating sample magnetometer with a noise level of about 10^{-9} Am^2 and a maximum applied field of 1 T. Hysteresis loops allow the determination of coercivity (B_C), saturation magnetization (M_S), saturation remanent magnetization (M_{RS}), high-field susceptibility (χ_{HF} , including both diamagnetic and paramagnetic contributions). Coercivity of remanence (B_{CR}) was evaluated through DC back-field demagnetization of the saturation remanence. The magnetic measurements were conducted at CEREGE.

X-ray diffraction (XRD) powder patterns were obtained using the D8 Discover Bruker diffractometer equipped with Cu-K α tube, nickel filter, and lynxeye detector located at Pontifícia Universidade Católica (PUC), Rio de Janeiro. The data were collected from 2 θ 10 to 90° with step-size and scan rate of 0.02° and 2.5 s per step, respectively. Refinement of the XRD data were performed using the Bruker TOPAS 4.2[®] program with the fundamental parameters approach. Up to 18 different phases were considered during the Rietveld modeling. The phases were considered stoichiometric or with constant composition. The residual weighted pattern and the goodness of fitting (χ^2) were always smaller than 5.6 and 1.6, respectively.

Chemical compositions of the mineral phases were determined with CAMECA SXFive and SX100 electron microprobes at the CAMPARIS facility (Paris), using natural and synthetic standards, focused electron beam (~1 μm in diameter), an accelerating voltage of 15 kV, and a beam current of 10 nA.

Between 80 and 100 mg of powdered sample were used to measure loss on ignition (LOI) contents on selected meteorites. Samples were heated up to 110, 550, and 850 °C, for 30, 60, and 60 min, respectively. Sample weighting followed 10 min of equilibration into a desiccator.

The total carbon (TC), total organic carbon (TOC), and total nitrogen were measured with a FISONs NA

1500 elemental analyzer (Carlo Erba NA-1500 Elemental Analyser) at CEREGE, as described in Pailler and Bard (2002) and Soulet et al. (2011). Selected meteorite samples were crushed and homogenized in an agate ball mill. Aliquots of 10–20 mg of the powders were loaded in aluminum cups. The TC, nitrogen, and the TOC contents of each sample were determined in two separate analyses. We measured TOC after an acid removal (using sulfurous acid) of the carbonate fraction. Each TOC measurement was duplicated. In order to calculate the dry weight percentages of calcium carbonate, the following equation was applied: $\text{CaCO}_3 = (\text{TC} - \text{TOC}) \times 8.33$. In the course of the measurements, acetanilide ($\text{C}_8\text{H}_9\text{NO}$) was used as standard.

For major element analysis, the whole rock powders of selected meteorites were digested by the alkali fusion method using lithium tetraborate. The analysis were carried out using an Ultima-C, Jobin Yvon, Horiba induced coupled plasma–atomic emission spectroscopy at CEREGE.

The trace element contents of the selected meteorite samples were determined by inductively coupled plasma–mass spectrometry (ICP-MS; Perkin-Elmer NexION[®] 300×) at the Pisa University's Dipartimento di Scienze della Terra. About 50–100 mg of each whole rock powder was dissolved in a mixture of HF and HNO_3 on a hot plate at ~ 120 °C inside screw-top perfluoroalkoxy vessels. Then, the sample solutions were spiked with Rh, Re, and Bi as internal standards (20 ng mL^{-1} in the final solutions) and diluted to 50 mL in polypropylene flasks. In each step of sample preparation, Milli-Q[®] purified water ($18.2 \text{ M}\Omega \text{ cm}$), ultrapure HF, and HNO_3 were used. The correction procedure included (1) blank subtraction, (2) instrumental drift correction using internal standardization and repeated (every five samples) analysis of a drift monitor, and (3) oxide-hydroxide interference correction. The geochemical reference samples with basaltic composition WS-E and PM-S, and the Allende chondrite reference sample (USNM 3529, split 20, position 22) dissolved and analyzed along with the unknown samples to check the accuracy of the results.

Soil samples from three different locations in Kalut were also collected in order to analyze the trace element contents. Around 50 mg of crushed samples were dissolved by alkali fusion using a mixture of lithium metaborate and lithium tetraborate. Samples were measured at the Université Libre de Bruxelles on an ICP-MS Agilent 7700, with In as an internal standard. Reference geological materials (BHVO and AGV) were used to assess the external reproducibility. The relative standard deviation (2RSD) was generally better than 5%.

Three samples from different meteorites were sent to the University of Arizona AMS Laboratory in order to estimate the terrestrial age, using the protocol of Jull et al. (1993, 2010). Samples were crushed, pretreated with 85% phosphoric acid to remove weathering products, washed in distilled water, and dried. The meteorite powder (~ 0.2 to 0.3 g) is mixed with $\sim 3 \text{ g}$ of iron chips, which are a combustion accelerator. The mixture is placed in a ceramic crucible and preheated to 500 °C to remove organic contaminants. The crucible is then placed in an RF furnace (Jull et al. 2010) and the sample heated to melting for 2 min in a flow of oxygen. The recovered gases are converted to CO_2 through a CuO–CeO furnace and recovered from the oxygen flow cryogenically. CO_2 is converted to graphite using standard methods at Arizona and measured by accelerator mass spectrometry.

METEORITES COLLECTED IN THE LUT DESERT

Classification

Classification was based on optical microscopic observations, magnetic measurements, and chemical analyses of olivine and low-Ca pyroxene. Magnetic susceptibility (χ) is a proxy to differentiate various groups of meteorites and/or to estimate weathering grade (Rochette et al. 2003, 2008, 2009). Magnetic susceptibility can be used to classify and pair meteorites (e.g., Rochette et al. 2003; Folco et al. 2006; Smith et al. 2006; Debaille et al. 2017). This applies both to fresh and weathered desert meteorites (Rochette et al. 2012; Munayco et al. 2013).

The list of the meteorites classified during this work along with their classification data are reported in Table 1. In addition to the meteorites classified by us, the other Lut meteorites are also included in this table. So far, all of the collected and classified meteorites from the Lut are OCs. Figure 3 shows macroscopic and microscopic images of H5 and L5 chondrites, the two most common types of meteorites collected in the Lut Desert. The classification of these OCs is discussed in the following.

Among the Lut samples with approved names in the Meteoritical Bulletin ($n = 236$ as of February 2019), the majority ($n = 198$) are H5 (collected mostly in the Kerman DCA). Moreover, hundreds of additional probable H5 fragments have been recovered but are not officially classified. These unclassified samples and samples classified by other groups are not discussed in this part of the paper. Petrography, magnetic susceptibility, and spatial distribution of the meteorites (see the Meteorite Spatial Distribution section) suggest that most of these H5 meteorites from the Kerman DCA are paired, revealing the existence of a large H5

Table 1. The list of the classified meteorites from the Lut Desert. The majority of these meteorites were classified during this work. Meteorites classified by the other workers are shown inside parentheses.

Name	Latitude	Longitude	Mass (g)	Pieces	Class	Weathering	Fa (mole%)	Fs (mole%)	Wo (mole%)	Mag. Sus.
(Gandom Beryan ¹)	31°52.31'N	57°03.31'E	3927	5	L3	W1	20.3 ± 6.9 (N = 27)	17.9 ± 13.3 (N = 25)	1.8 ± 2.2	n.d.
(Gandom Beryan 002 ²)	31°52.73'N	57°3.83'E	1070	1	H4	W3	16.1 ± 0.2 (N = 5)	14.8 ± 0.9 (N = 5)	0.8 ± 0.1	n.d.
Gandom Beryan 003 ²	31°1.133'N	58°1.367'E	177	1	H5	W2	n.d.	n.d.	n.d.	4.79
Gandom Beryan 004 ²	31°12.567'N	58°8.783'E	6400	1	H5	W3	19.1 (N = 1)	17.8 (N = 1)	1.5	4.76
Gandom Beryan 005 ²	31° 51.983'N	57° 3.567'E	2510	5	H5	W3	17.9 (N = 1)	16.2 (N = 1)	1.1	4.67
Gandom Beryan 006 ²	31° 53.650'N	57° 2.833'E	2000	110	H5	W4	18.1 (N = 2)	n.d.	n.d.	4.87
Gandom Beryan 007 ²	31° 52.783'N	57° 6.583'E	1430	27	H5	W2	18.6 (N = 1)	16.1 (N = 1)	1.1	4.91
(Gandom Beryan 008 ²)	31°53'15.24"N	57° 2'28.08"E	11000	Many	H5	W3-4	18.42 ± 0.45 (N = 41)	16.31 ± 0.52 (N = 43)	1.05 ± 0.19	n.d.
(Gandom Beryan 009 ²)	31°52'50.10"N	57°10'54.06"E	218	2	H5	W3-4	19.85 ± 0.11 (N = 41)	17.20 ± 0.26 (N = 47)	1.14 ± 0.24	n.d.
(Gandom Beryan 010 ³)	31°52.29'N	57°3.80	150	1	H5	W3	18.9 ± 0.8 (N = 10)	16.6 ± 0.9 (N = 10)	1.1 ± 0.4	n.d.
(Gandom Beryan 011 ³)	31°52.659' N	57°02.920' E	2067	1	LL3	W2	23.9 ± 7.4 (N = 141)	14.9 ± 8.1 (N = 70)	1.96 ± 1.85	n.d.
Kerman 001 ⁴	30°30.1'N	58°24.2'E	17000	1	H5	W4	18.4 ± 0.2 (N = 4)	16.4 ± 0.3 (N = 4)	1.1 ± 0.1	4.67
Kerman 002 ⁴	30°47.33'N	57°47.36'E	211	1	L6	W3	24.8 ± 0.1 (N = 2)	21.3 (N = 1)	1.6	4.63
Kerman 003 ⁵	30° 26.80'N	58° 27.00'E	615	1	L5	W2	25.3 ± 0.2 (N = 4)	22.0 ± 0.2 (N = 4)	1.9 ± 0.8	4.52
Kerman 004 ¹	30°45.614'N	57°47.690'E	70	2	H5	W3	18.9 (N = 1)	16.2 (N = 1)	1.4	4.6
Kerman 005 ¹	30°46.845'N	57°46.949'E	333	105	H5	W3	18.6 (N = 1)	17.2 (N = 1)	1.3	4.6
Kerman 006 ¹	30°46.047'N	57°47.475'E	220	10	H5	W3	18.9 (N = 1)	16.4 (N = 1)	1.4	4.63
Kerman 007 ¹	30°46.777'N	57°47.591'E	176	32	H5	W2	18.9 (N = 1)	16.9 (N = 1)	2	4.52
Kerman 008 ¹	30°45.162'N	57°48.287'E	20	2	H5	W4	18.7 (N = 1)	16.3 (N = 1)	1.3	4.61
Kerman 009 ¹	30°45.947'N	57°47.424'E	132	15	H5	W2	18.3 (N = 1)	16.5 (N = 1)	1.1	4.55
Kerman 010 ¹	30°46.726'N	57°47.371'E	105	5	H5	W3	18.5 (N = 1)	16.5 (N = 1)	1.3	4.45
Kerman 011 ¹	30°45.864'N	57°47.342'E	155	10	H5	W2	18.7 (N = 1)	18.1 (N = 1)	1.1	4.5
Kerman 012 ¹	30°46.188'N	57°47.498'E	494	34	H5	W4	19.0 (N = 1)	16.4 (N = 1)	1.2	4.63
Kerman 013 ¹	30°46.041'N	57°47.870'E	282	15	H5	W3	18.2 (N = 1)	16.1 (N = 1)	1.2	4.6
Kerman 014 ¹	30°45.348'N	57°48.213'E	604	30	H5	W3/4	18.6 (N = 1)	18.3 (N = 1)	1.2	4.48
Kerman 015 ¹	30°45.379'N	57°48.151'E	168	2	H5	W3	18.4 (N = 1)	16.4 (N = 1)	1.4	4.7
Kerman 016 ¹	30°46.142'N	57°47.411'E	33	2	H5	W3	18.4 (N = 1)	16.3 (N = 1)	1.5	4.61
Kerman 017 ¹	30°45.867'N	57°47.363'E	26	2	H5	W3	18.9 (N = 1)	16.3 (N = 1)	1.3	4.53
Kerman 018 ¹	30°46.879'N	57°46.767'E	16	1	H5	W3	18.6 (N = 1)	18.3 (N = 1)	0.6	4.42
Kerman 019 ¹	30°45.467'N	57°48.296'E	92	12	H5	W4	17.0 (N = 1)	20.2 (N = 1)	0.1	4.58

Table 1. *Continued.* The list of the classified meteorites from the Lut Desert. The majority of these meteorites were classified during this work. Meteorites classified by the other workers are shown inside parentheses..

Name	Latitude	Longitude	Mass (g)	Pieces	Class	Weathering	Fa (mole%)	Fs (mole%)	Wo (mole%)	Mag. Sus.
Kerman 020 ¹	30°45.349'N	57°48.214'E	620	60	H5	W4	19.3 (N = 1)	16.4 (N = 1)	1.2	4.55
Kerman 021 ¹	30°45.300'N	57°47.839'E	32	6	H5	W4	18.8 (N = 1)	16.5 (N = 1)	1.2	4.78
Kerman 022 ¹	30°45.576'N	57°48.005'E	98	5	H5	W2/3	18.6 (N = 1)	16.2 (N = 1)	1.4	4.55
Kerman 023 ¹	30°45.464'N	57°48.109'E	134	9	H5	W3	18.5 (N = 1)	16.9 (N = 1)	1.3	4.59
Kerman 024 ¹	30°48.424'N	57°45.240'E	16	1	L6	W2	24.3 (N = 1)	21.2 (N = 1)	1	4.06
Kerman 025 ¹	30°46.878'N	57°46.767'E	13	3	H5	W2/3	16.7 (N = 1)	18.0 (N = 1)	0	4.74
Kerman 026 ¹	30°47.795'N	57°46.500'E	4	1	L6	W2	24.2 (N = 1)	20.8 (N = 1)	1.6	4.5
Kerman 027 ¹	30°45.985'N	57°47.531'E	180	8	H5	W4	18.3 (N = 1)	16.2 (N = 1)	1.3	4.65
Kerman 028 ¹	30°38.008'N	57°50.023'E	7360	22	H5	W2	18.3 (N = 1)	17.3 (N = 1)	1	4.54
Kerman 029 ¹	30°45.149'N	57°48.516'E	170	12	H3	W2	17.7 ± 4.7 (N = 9)	12.9 ± 4.9 (N = 10)	0.9 ± 0.4	4.7
Kerman 030 ¹	30°45.565'N	57°47.961'E	200	32	H5	W4	18.5 (N = 1)	16.1 (N = 1)	0	4.6
Kerman 031 ¹	30°45.545'N	57°47.934'E	150	14	H5	n.d.	18.5 (N = 2)	16.0 (N = 2)	1.3	4.82
Kerman 032 ¹	30°51.658'N	57°46.802'E	2900	1	L6	W2	23.8 (N = 1)	21.0 (N = 1)	1.4	4.49
Kerman 033 ¹	30°52.439'N	57°48.621'E	2630	1	H5	W3	n.d.	15.6 (N = 1)	1.2	4.69
Kerman 034 ¹	30°51.983'N	57°48.620'E	720	1	H5	W1/W3	18.4 (N = 1)	16.5 (N = 1)	1.3	4.97
Kerman 035 ¹	30°45.760'N	57°47.689'E	110	3	H5	W3	18.6 (N = 1)	n.d.	n.d.	4.59
Kerman 036 ¹	30°45.948'N	57°47.891'E	65	4	H5	W3	19.5 (N = 1)	17.2 (N = 1)	1.4	4.53
Kerman 037 ¹	30°45.411'N	57°48.149'E	85	10	H5	W3	18.0 (N = 2)	16.1 (N = 1)	1.4	4.58
Kerman 038 ¹	30°45.482'N	57°47.942'E	120	10	H5	W2/3	18.5 (N = 1)	16.0 (N = 1)	1.6	4.63
Kerman 039 ¹	30°45.427'N	57°47.740'E	155	12	H5	W3	n.d.	17.0 (N = 3)	1.7	4.54
Kerman 040 ¹	30°45.568'N	57°48.256'E	40	2	H5	W3/4	19.2 (N = 3)	18.7 (N = 2)	0.7	4.54
Kerman 041 ¹	30°46.302'N	57°47.201'E	1210	20	H5	W2	18.6 (N = 1)	16.5 (N = 1)	1.3	4.51
Kerman 042 ¹	30°43.956'N	57°48.971'E	2300	57	H5	W2	18.9 (N = 1)	17.1 (N = 2)	1.4	4.58
Kerman 043 ¹	30°45.150'N	57°48.035'E	44	1	H5	W2	19.4 (N = 1)	n.d.	n.d.	4.58
Kerman 044 ¹	30°46.726'N	57°47.371'E	64	3	H5	W2	19.0 (N = 1)	16.6 (N = 1)	1.3	4.6
Kerman 045 ¹	30°44.561'N	57°47.996'E	7	1	LL6	W2	28.7 (N = 1)	n.d.	n.d.	3.75
Kerman 046 ¹	30°48.366'N	57°45.254'E	819	38	H5	W3	n.d.	n.d.	n.d.	4.53
Kerman 047 ¹	30°46.424'N	57°47.413'E	82	12	H5	W3	n.d.	n.d.	n.d.	4.56
Kerman 048 ¹	30°45.806'N	57°47.342'E	302	47	H5	W3	n.d.	n.d.	n.d.	4.55
Kerman 049 ¹	30°46.471'N	57°47.135'E	172	1	H5	W3	n.d.	n.d.	n.d.	4.56
Kerman 050 ¹	30°45.382'N	57°48.193'E	38	5	H5	W3	n.d.	n.d.	n.d.	4.55
Kerman 051 ¹	30°45.787'N	57°48.334'E	97	5	H5	W3	n.d.	n.d.	n.d.	4.59
Kerman 052 ¹	30°45.487'N	57°47.661'E	73	16	H5	W3	n.d.	n.d.	n.d.	4.57
Kerman 053 ¹	30°45.396'N	57°48.163'E	434	8	H5	W3	n.d.	n.d.	n.d.	4.6
Kerman 054 ¹	30°45.874'N	57°48.061'E	54	7	H5	W4	n.d.	n.d.	n.d.	4.63
Kerman 055 ¹	30°45.832'N	57°47.433'E	60	5	H5	W3	n.d.	n.d.	n.d.	4.5
Kerman 056 ¹	30°45.546'N	57°48.387'E	139	8	H5	W3	n.d.	n.d.	n.d.	4.54
Kerman 057 ¹	30°45.933'N	57°48.292'E	58	11	H5	W3	n.d.	n.d.	n.d.	4.58

Table 1. *Continued.* The list of the classified meteorites from the Lut Desert. The majority of these meteorites were classified during this work. Meteorites classified by the other workers are shown inside parentheses..

Name	Latitude	Longitude	Mass (g)	Pieces	Class	Weathering	Fa (mole%)	Fs (mole%)	Wo (mole%)	Mag. Sus.
Kerman 058 ¹	30°46.482'N	57°47.917'E	133	4	H5	W2	n.d.	16.3 (N = 1)	1.4	4.56
Kerman 059 ¹	30°45.525'N	57°48.562'E	303	24	H5	W2	n.d.	17.7 (N = 2)	1.2	4.45
Kerman 060 ¹	30°44.863'N	57°47.484'E	50	6	H5	W3	n.d.	n.d.	n.d.	4.51
Kerman 061 ¹	30°46.353'N	57°47.393'E	71	1	H5	W3	n.d.	n.d.	n.d.	4.68
Kerman 062 ¹	30°46.078'N	57°47.460'E	187	7	H5	W3	n.d.	n.d.	n.d.	4.64
Kerman 063 ¹	30°45.336'N	57°48.416'E	30	2	H5	W2	n.d.	n.d.	n.d.	4.78
Kerman 064 ¹	30°45.472'N	57°47.946'E	39	6	H5	W2/3	n.d.	n.d.	n.d.	4.52
Kerman 065 ¹	30°46.277'N	57°47.352'E	45	3	H5	W4	n.d.	n.d.	n.d.	4.65
Kerman 066 ¹	30°44.860'N	57°47.852'E	9	1	H5	W3	n.d.	n.d.	n.d.	4.65
Kerman 067 ¹	30°46.254'N	57°47.369'E	45	5	H5	W3	n.d.	n.d.	n.d.	4.59
Kerman 068 ¹	30°47.315'N	57°46.700'E	362	124	H5	W4	19.0 (N = 1)	17.0 (N = 1)	1.44	4.7
Kerman 069 ¹	30°45.838'N	57°48.527'E	45	6	H5	W3	n.d.	n.d.	n.d.	4.56
Kerman 070 ¹	30°45.218'N	57°48.034'E	49	16	H5	W3	n.d.	n.d.	n.d.	4.62
Kerman 071 ¹	30°46.005'N	57°47.582'E	50	3	H6	W3	n.d.	n.d.	n.d.	4.63
Kerman 072 ¹	30°45.755'N	57°47.480'E	59	2	H5	W3	n.d.	n.d.	n.d.	4.5
Kerman 073 ¹	30°46.325'N	57°47.306'E	95	2	H5	W4	n.d.	n.d.	n.d.	4.66
Kerman 074 ¹	30°45.659'N	57°48.381'E	240	10	H5	W3	n.d.	n.d.	n.d.	4.53
Kerman 075 ¹	30°45.722'N	57°48.524'E	134	2	H5	W2	n.d.	n.d.	n.d.	4.54
Kerman 076 ¹	30°45.590'N	57°48.415'E	55	3	H5	W3	n.d.	n.d.	n.d.	4.56
Kerman 077 ¹	30°44.702'N	57°48.253'E	50	7	H5	W3	n.d.	n.d.	n.d.	4.56
Kerman 078 ¹	30°46.038'N	57°48.533'E	21	3	H5	W3	n.d.	n.d.	n.d.	4.64
Kerman 079 ¹	30°45.737'N	57°48.253'E	172	7	H5	W3	n.d.	n.d.	n.d.	4.61
Kerman 080 ¹	30°45.978'N	57°47.298'E	70	15	H5	W3	n.d.	n.d.	n.d.	4.53
Kerman 081 ¹	30°46.494'N	57°47.423'E	60	6	H5	W3	n.d.	n.d.	n.d.	4.58
Kerman 082 ¹	30°45.600'N	57°47.876'E	18	1	H5	W3	n.d.	n.d.	n.d.	4.53
Kerman 083 ¹	30°45.738'N	57°48.264'E	43	12	H5	W3	n.d.	n.d.	n.d.	4.61
Kerman 084 ¹	30°45.824'N	57°48.438'E	62	4	H5	W3	n.d.	n.d.	n.d.	4.63
Kerman 085 ¹	30°45.748'N	57°48.253'E	36	1	H5	W2	n.d.	n.d.	n.d.	4.69
Kerman 086 ¹	30°47.411'N	57°46.779'E	15	1	H5	W3	n.d.	n.d.	n.d.	4.49
Kerman 087 ¹	30°46.084'N	57°47.444'E	45	2	H5	W2	n.d.	n.d.	n.d.	4.6
Kerman 088 ¹	30°44.992'N	57°48.669'E	12	1	H5	W2	n.d.	n.d.	n.d.	4.78
Kerman 089 ¹	30°45.701'N	57°48.263'E	33	4	H5	W2	n.d.	n.d.	n.d.	4.76
Kerman 090 ¹	30°45.742'N	57°48.270'E	27	4	H5	W4	n.d.	n.d.	n.d.	4.6
Kerman 091 ¹	30°45.667'N	57°48.452'E	7	1	H5	W2	n.d.	n.d.	n.d.	4.62
Kerman 092 ¹	30°47.411'N	57°46.779'E	8.5	3	H5	W4	19.4 (N = 1)	17.0 (N = 1)	1.4	4.68
Kerman 093 ¹	30°46.135'N	57°47.193'E	52	2	H5	W3	n.d.	n.d.	n.d.	4.49
Kerman 094 ¹	30°46.224'N	57°47.381'E	22	2	H5	W3	n.d.	n.d.	n.d.	4.52
Kerman 095 ¹	30°46.263'N	57°47.459'E	52	3	H5	W3	n.d.	n.d.	n.d.	4.46
Kerman 096 ¹	30°47.538'N	57°46.654'E	20	24	H5	W4	n.d.	n.d.	n.d.	4.55

Table 1. *Continued.* The list of the classified meteorites from the Lut Desert. The majority of these meteorites were classified during this work. Meteorites classified by the other workers are shown inside parentheses..

Name	Latitude	Longitude	Mass (g)	Pieces	Class	Weathering	Fa (mole%)	Fs (mole%)	Wo (mole%)	Mag. Sus.
Kerman 097 ¹	30°47.534'N	57°46.671'E	82	7	H5	W4	19.3 (N = 1)	17.0 (N = 1)	1.2	4.75
Kerman 098 ¹	30°46.424'N	57°47.942'E	26	3	H5	W3	n.d.	n.d.	n.d.	4.56
Kerman 099 ¹	30°46.878'N	57°46.775'E	8	5	H5	W3	n.d.	n.d.	n.d.	4.58
Kerman 100 ¹	30°45.684'N	57°48.664'E	31	5	H5	W2/3	n.d.	n.d.	n.d.	4.42
Kerman 101 ¹	30°44.448'N	57°48.309'E	31	6	H5	W4	n.d.	n.d.	n.d.	4.57
Kerman 102 ¹	30°45.711'N	57°48.228'E	7	1	H5	W3	n.d.	n.d.	n.d.	4.59
Kerman 103 ¹	30°45.281'N	57°48.029'E	52	3	H5	W3	n.d.	n.d.	n.d.	4.64
Kerman 104 ¹	30°45.899'N	57°48.382'E	21	3	H5	W3	n.d.	n.d.	n.d.	4.53
Kerman 105 ¹	30°46.107'N	57°47.423'E	34	1	H5	W3	n.d.	n.d.	n.d.	4.65
Kerman 106 ¹	30°46.419'N	57°47.276'E	116	5	H5	W3	n.d.	n.d.	n.d.	4.65
Kerman 107 ¹	30°45.692'N	57°48.383'E	72	6	H5	W3/4	n.d.	n.d.	n.d.	4.47
Kerman 108 ¹	30°46.327'N	57°47.338'E	20	1	H5	W3	17.3 (N = 1)	17.4 (N = 1)	1	4.72
Kerman 109 ¹	30°47.538'N	57°46.654'E	12	6	H5	W4	n.d.	n.d.	n.d.	4.5
Kerman 110 ¹	30°44.631'N	57°47.999'E	9.3	1	H5	W3	n.d.	n.d.	n.d.	4.63
Kerman 111 ¹	30°46.074'N	57°47.439'E	95	3	H5	W3	n.d.	n.d.	n.d.	4.64
Kerman 112 ¹	30°46.094'N	57°47.450'E	28	5	H5	W3/4	n.d.	n.d.	n.d.	4.49
Kerman 113 ¹	30°45.757'N	57°48.251'E	33	7	H5	W3	n.d.	n.d.	n.d.	4.61
Kerman 114 ¹	30°44.986'N	57°47.353'E	48	2	H5	W4	n.d.	n.d.	n.d.	4.55
Kerman 115 ¹	30°45.948'N	57°47.515'E	6.5	3	H5	W4	n.d.	n.d.	n.d.	4.69
Kerman 116 ¹	30°47.228'N	57°46.713'E	8.3	2	H5	W4	n.d.	n.d.	n.d.	4.68
Kerman 117 ¹	30°45.963'N	57°47.551'E	59	10	H5	W3	n.d.	n.d.	n.d.	4.65
Kerman 118 ¹	30°45.331'N	57°48.603'E	46	3	H5	W3	n.d.	n.d.	n.d.	4.66
Kerman 119 ¹	30°45.586'N	57°48.330'E	29	2	H5	W3	n.d.	n.d.	n.d.	4.45
Kerman 120 ¹	30°45.268'N	57°48.081'E	48	10	H5	W4	n.d.	n.d.	n.d.	4.55
Kerman 121 ¹	30°44.686'N	57°47.978'E	9.2	1	H5	W3	n.d.	n.d.	n.d.	4.68
Kerman 122 ¹	30°45.751'N	57°48.262'E	38	5	H5	W3	n.d.	n.d.	n.d.	4.53
Kerman 123 ¹	30°45.667'N	57°48.301'E	64	7	H5	W4	n.d.	n.d.	n.d.	4.62
Kerman 124 ¹	30°44.288'N	57°46.239'E	8	1	H5	W3	n.d.	n.d.	n.d.	4.52
Kerman 125 ¹	30°45.281'N	57°48.668'E	38	3	H5	W2	n.d.	n.d.	n.d.	4.71
Kerman 126 ²	30°47.516'N	57°47.850'E	65	2	H5	W2	n.d.	n.d.	n.d.	5.18
Kerman 127 ²	30°56.878'N	57°39.283'E	181	9	H5	W3	n.d.	n.d.	n.d.	4.52
Kerman 128 ²	30°47.317'N	57°54.017'E	813	2	H5	W2/3	n.d.	n.d.	n.d.	4.95
Kerman 129 ²	30°47.650'N	57°45.333'E	191	3	H5	W3	n.d.	n.d.	n.d.	4.47
Kerman 130 ²	30°49.109'N	57°49.218'E	65	2	H5	W2/3	n.d.	n.d.	n.d.	4.54
Kerman 131 ²	30°50.199'N	57°51.417'E	136	1	H5	W3	n.d.	n.d.	n.d.	4.58
Kerman 132 ²	30°45.583'N	57°49.383'E	96	1	H5	W3/4	n.d.	n.d.	n.d.	4.55
Kerman 133 ²	30°45.499'N	57°47.600'E	79	2	H5	W3	n.d.	n.d.	n.d.	4.57
Kerman 134 ²	30°53.482'N	58°1.250'E	174	11	H5	W3	n.d.	n.d.	n.d.	4.63
Kerman 135 ²	30°48.938'N	57°41.007'E	5749	1	H5	W2	19.7 (N = 1)	16.9 (N = 1)	1.1	4.69

Table 1. *Continued.* The list of the classified meteorites from the Lut Desert. The majority of these meteorites were classified during this work. Meteorites classified by the other workers are shown inside parentheses..

Name	Latitude	Longitude	Mass (g)	Pieces	Class	Weathering	Fa (mole%)	Fs (mole%)	Wo (mole%)	Mag. Sus.
Kerman 136 ²	30°45.117'N	57°46.047'E	28	1	H5	W2	18.5 (N = 1)	16.9 (N = 1)	1.3	4.75
Kerman 137 ²	30°39.632'N	57°51.754'E	130	1	L5	W1/2	24.8 (N = 1)	20.7 (N = 1)	1.6	4.63
Kerman 138 ²	30°39.262'N	57°52.023'E	1009	2	L5	W2/3	24.8 (N = 1)	21.0 (N = 1)	1.6	4.4
Kerman 139 ²	30°38.441'N	57°52.750'E	246	1	L5	W2	25.4 (N = 3)	20.9 (N = 2)	1.6	4.53
Kerman 140 ²	30°40.136'N	57°52.540'E	341	1	L5	W2	25.4 (N = 2)	21.4 (N = 1)	1.4	4.47
Kerman 141 ²	30°40.233'N	57°48.670'E	1630	2	L5	W1/2	25.4 (N = 2)	20.9 (N = 1)	1.5	4.2
Kerman 142 ²	30°39.707'N	57°49.403'E	2498	1	L5	W1/2	25.4 (N = 1)	20.5 (N = 1)	1.3	4.45
Kerman 143 ²	30°47.836'N	57°46.317'E	26	1	H5	W3	18.8 (N = 1)	17.0 (N = 1)	1.2	4.64
Kerman 144 ²	30°47.411'N	57°45.318'E	152	9	H5	W4	n.d.	n.d.	n.d.	4.75
Kerman 145 ²	30°47.618'N	57°47.463'E	205	4	H5	W3	n.d.	n.d.	n.d.	4.41
Kerman 146 ²	30°47.516'N	57°46.812'E	295	5	H5	W3	n.d.	n.d.	n.d.	4.67
Kerman 147 ²	30°46.716'N	57°46.119'E	25	1	H5	W3	n.d.	n.d.	n.d.	4.65
Kerman 148 ²	30°45.816'N	57°46.611'E	207	7	H5	W2	n.d.	n.d.	n.d.	4.58
Kerman 149 ²	30°47.219'N	57°46.431'E	143	3	H5	W2	n.d.	n.d.	n.d.	4.85
Kerman 150 ²	30°45.391'N	57°46.812'E	20	3	H5	W3	n.d.	n.d.	n.d.	4.65
Kerman 151 ²	30°47.881'N	57°46.319'E	300	3	H5	W2/3	n.d.	n.d.	n.d.	4.88
Kerman 152 ²	30°45.431'N	57°46.716'E	20	1	H5	W2/3	n.d.	n.d.	n.d.	4.56
Kerman 153 ²	30°40.439'N	57°47.504'E	1640	2	L5	W2/3	n.d.	n.d.	n.d.	4.32
Kerman 154 ²	30°39.353'N	57°48.454'E	1232	2	L5	W2	n.d.	n.d.	n.d.	4.21
Kerman 155 ²	30°41.225'N	57°48.969'E	200	1	L5	W2	n.d.	n.d.	n.d.	4.16
Kerman 156 ²	30°40.719'N	57°48.941'E	830	2	L5	W2	25.9 (N = 1)	20.7 (N = 1)	1.9	4.36
Kerman 157 ²	30°45.486'N	57°47.661'E	20.6	1	H5	W3	n.d.	n.d.	n.d.	4.57
Kerman 158 ²	30°44.219'N	57°46.171'E	25.5	1	H5	W3	n.d.	n.d.	n.d.	4.61
Kerman 159 ²	30°47.971'N	57°56.462'E	20	1	H5	W2	n.d.	n.d.	n.d.	4.64
Kerman 160 ²	30°45.877'N	57°48.312'E	291	14	H5	W3	n.d.	n.d.	n.d.	4.62
Kerman 161 ²	30°45.417'N	57°47.729'E	20.6	1	H5	W3	n.d.	n.d.	n.d.	4.59
Kerman 162 ²	30°45.511'N	57°47.936'E	33.5	1	H5	W3	n.d.	n.d.	n.d.	4.58
Kerman 163 ²	30°45.520'N	57°48.265'E	15.6	1	H5	W3/4	n.d.	n.d.	n.d.	4.64
Kerman 164 ²	30°44.712'N	57°46.118'E	23	1	H5	W2	n.d.	n.d.	n.d.	4.81
Kerman 165 ²	30°44.716'N	57°45.216'E	18	1	H5	W3/4	n.d.	n.d.	n.d.	4.66
Kerman 166 ²	30°45.693'N	57°47.221'E	13.6	1	H5	W3	n.d.	n.d.	n.d.	4.66
Kerman 167 ²	30°45.788'N	57°48.304'E	819	37	H5	W2/3	n.d.	n.d.	n.d.	4.58
Kerman 168 ²	30°44.533'N	57°48.593'E	22	1	H5	W2	n.d.	n.d.	n.d.	4.65
Kerman 169 ²	30°45.952'N	57°47.880'E	16	2	H5	W3	n.d.	n.d.	n.d.	4.6
Kerman 170 ²	30°45.118'N	57°48.473'E	68	3	H5	W3	n.d.	n.d.	n.d.	4.69
Kerman 171 ²	30°45.218'N	57°47.661'E	986	11	H5	W4	n.d.	n.d.	n.d.	4.65
Kerman 172 ²	30°47.816'N	57°46.374'E	17.5	1	H5	W3	n.d.	n.d.	n.d.	4.61
Kerman 173 ²	30°43.942'N	57°47.882'E	19.4	1	H5	W2	n.d.	n.d.	n.d.	4.62
Kerman 174 ²	30°45.721'N	57°46.107'E	23	1	H5	W2/3	n.d.	n.d.	n.d.	4.76

Table 1. *Continued.* The list of the classified meteorites from the Lut Desert. The majority of these meteorites were classified during this work. Meteorites classified by the other workers are shown inside parentheses..

Name	Latitude	Longitude	Mass (g)	Pieces	Class	Weathering	Fa (mole%)	Fs (mole%)	Wo (mole%)	Mag. Sus.
Kerman 175 ²	30°45.321'N	57°47.809'E	21	1	H5	W4	n.d.	n.d.	n.d.	4.59
Kerman 176 ²	30°45.408'N	57°48.133'E	13.6	1	H5	W3/4	n.d.	n.d.	n.d.	4.51
Kerman 177 ²	30°45.437'N	57°47.738'E	18	1	H5	W3	n.d.	n.d.	n.d.	4.54
Kerman 178 ²	30°45.712'N	57°47.413'E	18.5	1	H5	W3	n.d.	n.d.	n.d.	4.61
Kerman 179 ²	30°48.033'N	57°50.067'E	61	2	H5	W1-2	n.d.	n.d.	n.d.	4.79
Kerman 180 ²	30°46.900'N	57°50.433'E	114	2	H5	W3	n.d.	n.d.	n.d.	4.56
Kerman 181 ²	30°47.883'N	57°52.450'E	1987	1	H5	W2	n.d.	n.d.	n.d.	4.63
Kerman 182 ²	30°41.133'N	57°50.017'E	265	13	H5	W2	n.d.	n.d.	n.d.	4.66
Kerman 183 ²	30°48.067'N	57°50.050'E	67	1	H5	W3	n.d.	n.d.	n.d.	4.62
Kerman 184 ²	30°44.283'N	57°50.200'E	385	17	H5	W3	n.d.	n.d.	n.d.	4.71
Kerman 185 ²	30°46.517'N	57°52.450'E	935	110	H5	W3	n.d.	n.d.	n.d.	4.63
Kerman 186 ²	30°49.000'N	57°50.467'E	85	3	H5	W3	n.d.	n.d.	n.d.	4.61
Kerman 187 ²	30°46.467'N	57°52.500'E	2644	13	H5	W3	n.d.	n.d.	n.d.	4.59
Kerman 188 ²	30°42.067'N	57°48.467'E	251	4	H5	W3	n.d.	n.d.	n.d.	4.5
Kerman 189 ²	30°48.500'N	57°55.183'E	117	3	H5	W3	n.d.	n.d.	n.d.	4.56
Kerman 190 ²	30°53.933'N	57°59.250'E	69	2	H5	W3	n.d.	n.d.	n.d.	4.64
Kerman 191 ²	30°53.817'N	57°58.183'E	72	1	H5	W3	n.d.	n.d.	n.d.	4.61
Kerman 192 ²	30°51.500'N	57°48.417'E	120	4	H5	W3	n.d.	n.d.	n.d.	4.59
Kerman 193 ²	30°57.717'N	58°2.133'E	443	60	H5	W5	n.d.	n.d.	n.d.	4.71
Kerman 194 ²	30°59.983'N	58°1.483'E	222	2	H5	W3	n.d.	n.d.	n.d.	4.68
Kerman 195 ²	30°53.333'N	57°58.867'E	257	9	H5	W2	n.d.	n.d.	n.d.	4.58
Kerman 196 ²	30°53.800'N	57°42.700'E	40	1	H5	W2/3	n.d.	n.d.	n.d.	4.71
Kerman 197 ²	30°47.067'N	57°47.983'E	143	6	H5	W3	n.d.	n.d.	n.d.	4.65
Kerman 198 ²	30°45.801'N	57°47.911'E	43	6	H5	W4	n.d.	n.d.	n.d.	4.54
Kerman 199 ²	30°47.218'N	57°46.923'E	6.5	1	H5	W4	19.1 (N = 1)	17.0 (N = 1)	1.2	4.58
Kerman 200 ²	30°39.739'N	57°48.915'E	1700	2	L5	W2	n.d.	n.d.	n.d.	4.29
Kerman 201 ²	30°54.283'N	58°1.233'E	93	2	H5	W2	n.d.	n.d.	n.d.	4.62
Kerman 202 ²	30°54.917'N	57°59.600'E	68	2	H5	W2	n.d.	n.d.	n.d.	4.64
(Kerman 203 ²)	30°45'14.76"N	57°48'1.32"E	59	6	H5	W3-4	19.49 ± 0.38 (N = 61)	17.06 ± 0.47 (N = 52)	1.34 ± 0.17	n.d.
(Kerman 204 ³)	30°23.99'N	57°54.92'E	68	1	H5	W3	20.4 ± 0.2 (N = 6)	19.0 ± 0.3 (N = 6)	1.5 ± 0.1	n.d.
Lut-e-Zangi Ahmad 001 ²	29°48.667'N	59°11.667'E	290	1	H5	W1	19.5 (N = 1)	17.3 (N = 2)	1.26	5.07
(Lut-e-Zangi Ahmad 002 ²)	29°41.708'N	59°5.813'E	8634	1	L3	W3	22.2 ± 4.3 (N = 19)	16.7 ± 5.6 (N = 8)	1.8 ± 2.5	n.d.
Lut-e Zangi Ahmad 003 ³	29°43'17"N	58°50'26"E	300	4	L6	W3	25.5 (N = 1)	21.6 (N = 1)	1.8	4.44
(Lut 001 ⁴)	30°18.14'N	59°12.10'E	1030	52	H5	W3	18.2 ± 0.4 (N = 12)	n.d.	1.1 ± 1.2	n.d.

Table 1. *Continued.* The list of the classified meteorites from the Lut Desert. The majority of these meteorites were classified during this work. Meteorites classified by the other workers are shown inside parentheses..

Name	Latitude	Longitude	Mass (g)	Pieces	Class	Weathering	Fa (mole%)	Fs (mole%)	Wo (mole%)	Mag. Sus.
(Lut 002 ⁴)	30°17'26"N	59°23'55"E	568	1	H4	W3	17.0 ± 0.3	14.9 ± 0.2	1.2 ± 0.2	n.d.
(Lut 003 ⁴)	30°16'21"N	59°21'23"E	504	1	L3	W3	18.7 ± 8.2	16.1 ± 6.1	1.1 ± 0.7	n.d.
(Lut 004 ⁴)	30°16'23"N	59°21'36"E	505	1	H3	W3	21.8 ± 8.7	12.7 ± 10.2	1.1 ± 1.2	n.d.
(Lut 005 ⁴)	30°14'55"N	59°18'12"E	93	1	LL3	W3	24.6 ± 5.1	18.7 ± 9.2	1.1 ± 1.1	n.d.
(Lut 006 ⁴)	30°14'55"N	59°18'12"E	87	1	LL3	W3	23.7 ± 7.0	20.3 ± 8.2	2.2 ± 1.3	n.d.
(Lut 007 ⁴)	30°14'55"N	59°18'12"E	55	1	LL3	W3	23.9 ± 5.8	18.2 ± 7.8	0.6 ± 0.4	n.d.
Lut 008 ⁴	30°23.52'N	58°38.44'E	215	1	H4	W5	18.0 ± 0.2 (N = 4)	16.2 ± 0.1 (N = 3)	1.0 ± 0.1	4.71
Lut 009 ⁵	30°20.38' N	59°09.04' E	40.6	1	H4	W4	19.0 ± 0.7 (N = 31)	16.0 ± 3.0 (N = 31)	0.9	4.75
Lut 010 ⁵	30°28.038'N	59°23.183'E	926	10	LL6	W2-4	26.3 ± 0.8 (N = 5)	22.3 ± 0.4 (N = 3)	1.6 ± 0.2	4.18
Lut 011 ¹	30°55.02'N	59°46.07'E	750	2	L4	W2	22.8 ± 1(N = 4)	17.7 ± 1.5 (N = 4)	0.6 ± 0.8	4.64
Lut 012 ²	30°56.318'N	58°45.421'E	10311	1	L6	W2	25.3 (N = 1)	21.5 (N = 1)	1.3	4.42
(Lut 013 ²)	30°18.169'N	59°11.301'E	9406	1	H5	W2	17.3 ± 0.3 (N = 10)	15.6 ± 0.8 (N = 8)	1.2 ± 1.1	n.d.
(Lut 014 ²)	30°18.865'N	59°12.577'E	1030	52	H5	W2	17.9 ± 0.9 (N = 23)	16.0 ± 0.9 (N = 11)	1.4 ± 0.4 (N = 11)	n.d.
(Lut 015 ²)	30°19.323'N	59°19.002'E	37	1	L6	W1	24.3 ± 0.7 (N = 25)	20.6 ± 1.0 (N = 12)	1.8 ± 0.7	n.d.
(Lut 016 ²)	30°19.323'N	59°19.002'E	10	1	H4	W4	18.1 ± 0.8 (N = 29)	16 ± 1.2 (N = 12)	1.1 ± 0.5	n.d.
(Lut 017 ²)	30°19'N	59°19'E	24	1	H5	W2	17.5 ± 0.8 (N = 29)	15.7 ± 0.9 (N = 11)	1.1 ± 0.4 (N = 11)	n.d.
(Shahdad ⁶)	30°33.23'N	57°47.05'E	1074	1	H5	W4	18.4	n.d.	n.d.	n.d.

n.d. = not determined.
¹Bouvier et al. (2017b).
²Gattacceca et al. (2018).
³Gattacceca et al. (2019).
⁴Ruzicka et al. (2017).
⁵Bouvier et al. (2017a).
⁶Garvie (2012).

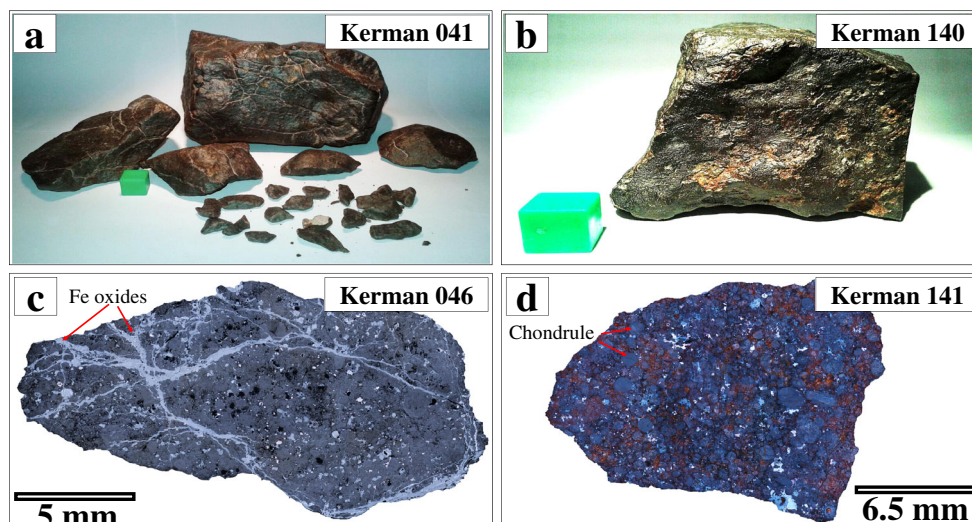


Fig. 3. Hand specimen and microscopic images (in reflected optical light) of meteorites from H5 and L5 strewnfields. a) Kerman 041 (H5, W2). Lack of fusion crust and the presence of a dark-brown desert patina is a common feature in Kerman paired H5 meteorites. Scale bar is 1×1 cm. b) Kerman 141 (L5, W2). The majority of Kerman paired L5 meteorites have a well-preserved fusion crust. c) Kerman 046 (H5, W3). Metal grains in Kerman paired H5 fragments are heavily altered to iron oxyhydroxides (light-gray areas). d) Kerman 141 (L5, W1/2). In comparison to Kerman paired H5 samples, paired L5 fragments have less weathering degrees and their chondritic texture is easily visible. Note the presence of white metal grains. (Color figure can be viewed at wileyonlinelibrary.com.)

strewnfield formed by a single meteorite fall event. This strewnfield is officially known as Shahdad strewnfield. The evidence for pairing is their similar petrographic features, a relatively narrow range of magnetic susceptibility (average $\log \chi = 4.60 \pm 0.12$, $n = 187$), and their spatial distribution.

Representative image of these paired H5 fragments is shown Fig. 3a. All of these samples have identical textures (Fig. 3c). Chondrules are readily delineated. Plagioclase with average size, about $15 \mu\text{m}$, is found in the interchondrule matrix. Most samples contain chromite-plagioclase assemblages. Melt veins and melt pockets are present. Relict troilite rims occur around some chondrules. Metal and troilite are well separated from each other. Metal and troilite are monocrystalline. In addition to petrographic data, these H5 meteorites have a narrow magnetic susceptibility range with an average $\log \chi = 4.60 \pm 0.12$ ($n = 187$).

The second most abundant meteorite type from Kerman DCA is L5 (Table 1) (Fig. 3b,d). The L5 fragments show a well-preserved chondritic texture. The complete separation of metal from troilite and average matrix plagioclase size below $50 \mu\text{m}$ indicate a petrologic type 5 (Van Schmus and Wood 1967). Similar to the H5 population, these meteorites are also paired, which indicates the existence of another strewnfield, whose minimum size is 8×7 km. Pairing of these samples is supported by their identical macroscopic features (e.g., fusion crust, color), textures (chondrule size, plagioclase

size, metal–troilite relationship, weathering degree, etc.), and magnetic susceptibilities (average $\log \chi = 4.37 \pm 0.15$, $n = 11$) (Table 1).

Meteorite Spatial Distribution

Meteorites have been collected from four DCAs defined in the Lut Desert. These DCAs, from highest to lowest number of the classified meteorites, include Kerman ($n = 205$, including Shahdad meteorite), Lut ($n = 17$), Gandom Beryan ($n = 11$), and Lut-e-Zangi Ahmad ($n = 3$) (Table 2). The Kerman DCA covers most of the Kalut area. Rig-e Yalan inside the Lut DCA is the second meteorite-rich region. The reason for the lower number of meteorites from the central hammada is the dark color of the local rocks, which makes it less attractive for meteorite hunting. Gandom Beryan DCA, which hosts the Gandom Beyran volcanic complex (Yousefi et al. 2017), is a well-known geotourism site attracting adventurers and leading to an increase in meteorite finding chance along their route.

Focusing on Kerman DCA and Kalut, Fig. 4a shows the spatial distribution of the Shahdad H5 strewnfield, located in the northwestern part of the Kalut, and the other collected meteorites. These H5 meteorites are found in an area of about 8×6 km. They do not appear spatially distributed as a function of mass (Fig. 4b). This indicates either a high-angle meteorite fall or a postimpact disturbance caused by

Table 2. Statistics of meteorite types and frequency in different DCAs from the Lut Desert.

DCA name	Meteorite type										Total meteorite number
	H3	H4	H5	H6	L3	L4	L5	L6	LL3	LL6	
Kerman	1	0	185	1	0	0	12	4	0	1	205
Lut	1	4		0	1	1	0	2	3	1	17
Gandom Beryan	0	1	8	0	1	0	0	0	1	0	11
Lut-e-Zangi Ahmad	0	0	1	0	1	0	0	1	0	0	3
											$\Sigma = 236$

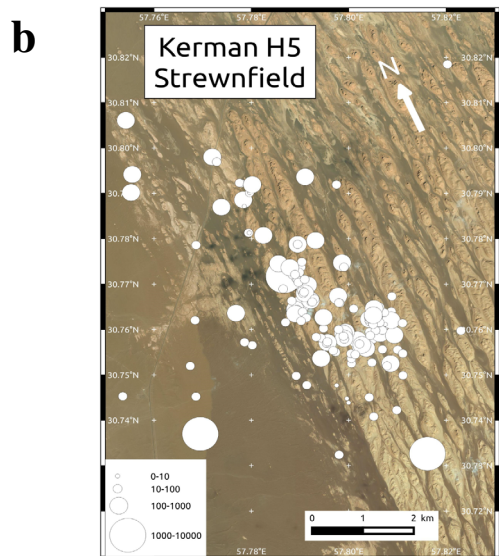
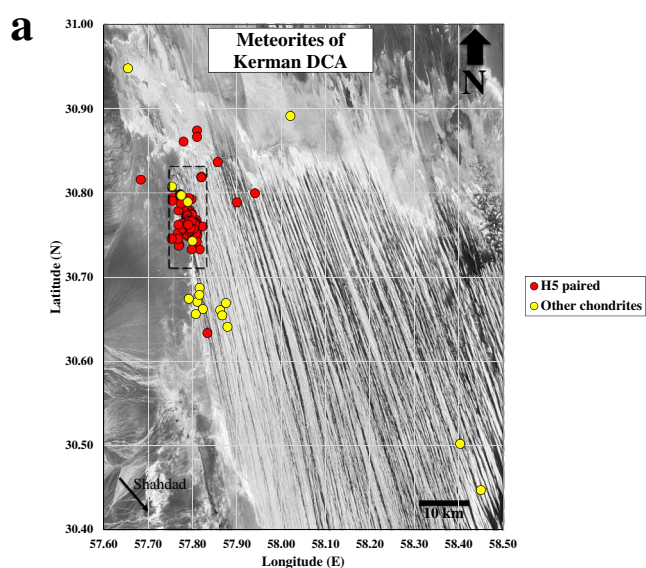


Fig. 4. a) Spatial distribution map of the Kerman DCA meteorites showing the paired H5 and other chondrites. Dashed area is showing the boundaries of (b). b) Location and mass (g) of the H5 paired fragments collected from Kalut. (Color figure can be viewed at wileyonlinelibrary.com.)

Table 3. Terrestrial ages of three selected Lut meteorites based on their ¹⁴C activities.

Meteorite	Type	¹⁴ C (dpm/kg)	Terrestrial age (kyr)
Kerman 001 ¹	H5, W4	8.16 ± 0.71	14.4 ± 1.5
Lut 006 ¹	LL3, W3	5.87 ± 0.30	18.5 ± 1.4
Lut 010 ²	LL6, W2-4	1.70 ± 0.33	28.8 ± 2.1

¹Ruzicka et al. (2017).

²Bouvier et al. (2017a).

floods, which is unlikely in view of the arid climate of the region. Total mass of these H5 fragments is 32.3 kg and the biggest fragment is 5750 g. The average and median masses are 270 and 64 g, respectively. The L5 paired samples have average and median masses of 1070 and 1000 g, respectively.

Terrestrial Ages

The terrestrial ages calculated from the ¹⁴C activities measured in three selected samples are reported in Table 3. The main reason for choosing these particular samples was to have a preliminary evaluation about the oldest terrestrial ages of strongly weathered OCs from two main DCAs of the Lut Desert (Kerman and Lut). These samples were collected from Kalut and Rig-e Yalan. Kerman 001 (H5) is a heavily weathered (W4) single piece (17 kg) from Kalut region, but not a part of H5 strewnfield (Ruzicka et al. 2017). Lut 006 is a heavily weathered (W3) LL3 from Rig-e Yalan region (Ruzicka et al. 2017). Lut 010 is a LL6 with variable weathering degrees (W2–W4) in different fragments (Bouvier et al. 2017a). However, the most weathered parts were chosen for analysis. Lut 006 and Lut 010 were found in the Rig-e Yalan region. There is no clear relation between the weathering grades and the terrestrial ages: the most weathered meteorite, Kerman 001 (W4), is also the youngest meteorite. Although the number of the analyzed samples is limited, the age range (14–30 kyr) is consistent with the values reported

for meteorites from other hot deserts such as deserts of United Arab Emirates (Hezel et al. 2011), Nullarbor region in Australia (Jull et al. 2010), and Dar al Gani region in Libya (Welten et al. 2004), except for the older Atacama Desert in Chile (Gattacceca et al. 2011).

TERRESTRIAL WEATHERING OF THE LUT DESERT METEORITES

Mineralogy and Texture

Petrography

Here, we present petrographic evidence for terrestrial weathering of paired H5 and L5 meteorites from the Lut Desert. The lack of fusion crust, the presence of a dark-brownish-colored desert patina with attached sand grains, orange to brownish color of the broken or cut surfaces, cracks filled by desert sediments, the elevated number of small fragments (<10 g), and the low number of metal and troilite grains, are common among the majority of the H5 samples (Fig. 3a,c). While cutting these samples, they break down easily to smaller fragments. All these observations point to the strong effects of terrestrial weathering on the texture and the mineralogy of these fragments. Microscopic survey of the paired H5 sections shows that in ~80% of them, between 60% and 95% of the metal and troilite grains are replaced by Fe oxyhydroxides (Table 1), indicating a weathering grade W3 using the scale of Wlotzka (1993). Weathering products occur as both veins and pockets (Fig. 3c). Both W2 and W4 meteorites have 10% abundance of the paired H5 population. Only one sample (Lut-e-Zangi Ahmad 001) with minor oxidation (W1) and $\log \chi = 5.07$ was recovered, which is from the Rig-e Yalan and based on petrographic differences such as the troilite shape and size, is not related to the Shahdad H5 strewnfield.

Unlike the paired Kerman H5, most L5 meteorites are fully or partially covered by fusion crust and are relatively fresh looking (Fig. 3b,d). Hygroscopic mineral products formed during the interaction of the meteorite with water in the desert environment are visible as bulging spots on the exterior of the meteorites. Similar to the “sweating” behavior of Omani OCs described by Zurfluh et al. (2013), the L5 meteorites show crystallization of hygroscopic mineral assemblages in the cut surfaces. Microscopically, the L5 samples are also less weathered than the H5 fragments, 82% of them being W2 (Table 1).

Comparison of the macroscopic and microscopic data of the paired L5 and paired H5 fragments shows a relatively higher degree of weathering for the H5 fragments. As mentioned, the majority of the H5 are W3 while L5 are mostly W2. Considering a similar

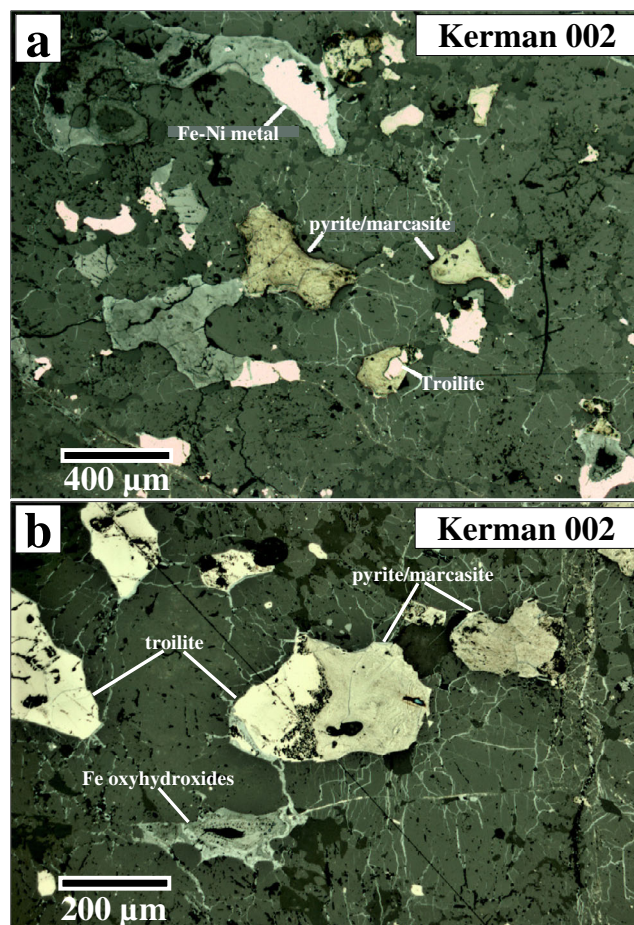


Fig. 5. Weathering of troilite to pyrite/marcasite visible in reflected light in a meteorite from the Lut Desert. (Color figure can be viewed at wileyonlinelibrary.com.)

climatic and geological characteristics for the fall area, lower weathering degree, and better preservation of L5, we suggest a lower terrestrial age for the L5 than the H5 fragments.

Troilite Weathering

In most samples from the Lut Desert, troilite has a higher modal abundance than metal, which indicates its higher resistance to weathering. Alteration of troilite to pyrite or marcasite is a ubiquitous characteristic of meteorites from Lut Desert, especially in the highly weathered ($\geq W3$) meteorites from Kalut (Fig. 5). Usually in desert meteorites with progressive weathering, in reaction with water, troilite releases sulfur as sulfuric acid, and the whole rock sulfur budget of the system decreases (Bland et al. 2006; Saunier et al. 2010). Subsequently, Fe oxyhydroxides replace the troilite grains. However, troilite weathering in the Lut Desert occurs in at least two steps. First troilite turns into pyrite or marcasite, indicating the presence of extra

sulfur and sulfuric acid (Schoonen and Barnes 1991; Hyde et al. 2014), and later to Fe oxyhydroxides. In addition to the Lut Desert meteorites, we have observed rare cases of similar phenomenon in OCs from Oman during the routine classification of meteorites in CEREGE. Al-Kathiri et al. (2005) and Hyde et al. (2014) also mention the alteration of troilite to pyrite and marcasite for Omani OCs and NWA 4872 brachinite, respectively.

Magnetic Properties

Oxidation of metal in meteorites affects their magnetic properties (Rochette et al. 2003; Uehara et al. 2012; Munayco et al. 2013). A decrease in the magnetic susceptibility compared to the average values for fresh and fall samples of each meteorite group is observed in the Lut Desert meteorites. With an average $\log \chi$ of 4.60 ± 0.10 ($n = 182$) compared to the average value of 5.32 ± 0.10 for H5 falls (Rochette et al. 2003), the paired H5 meteorites clearly show a significant effect of weathering. The same effect, although less intense, is observed for the paired L5 fragments. The average $\log \chi$ for the L5 fragments is 4.37 ± 0.15 ($n = 11$), which is lower than the fall L chondrites (4.90 ± 0.09) (Rochette et al. 2003). In agreement with meteorites from other hot deserts, magnetic susceptibility values of both H5 and L6 meteorites follow the same decreasing trend as those from Sahara (Rochette et al. 2003) and Atacama (Gattacceca et al. 2011) deserts. The average $\log \chi$ of the dominant W3 paired H5 meteorites is 4.59 ± 0.08 ($n = 118$). This is lower than the average 4.81 ± 0.17 ($n = 10$), but in range of the results for W3 H chondrites from San Juan region of the Atacama Desert as reported by Gattacceca et al. (2011) and meteorites from other parts of the Atacama Desert (Rochette et al. 2012). The same is true for the paired L5 (W2) chondrites, whose average $\log \chi$ 4.37 ± 0.15 ($n = 11$) is lower than San Juan L (W2) chondrites with average $\log \chi$ 4.59 ± 0.15 ($n = 6$). Differences in weathering regimes between the two deserts and different secondary mineralogy likely cause this effect.

The hysteresis properties of five meteorites from Kerman and Lut DCAs are presented in Table 4 and Fig. S3 in supporting information. Comparison with the data of Gattacceca et al. (2014) for fall OCs shows the mineralogical changes due to terrestrial weathering, in particular a strong increase in remanence and parameters typical of fine-grained (pseudo-single domain) cubic iron oxide (maghemite or magnetite), as already described in Uehara et al. (2012). M_s values, ranging from 2.4 to 5.5, indicate rather low amount of ferromagnetic minerals: 1–2 wt% in the case of metal, or 3–7 wt% percent in the case of maghemite-magnetite.

Table 4. Magnetic properties of selected ordinary chondrites from the Lut Desert.

Meteorite	Type	M_s^3				
		(A_m^2 /kg)	B_c^4 (mT)	B_{cr}^5 (mT)	M_{rs}^6 / M_s	B_{cr} / B_c
Kerman 001 ¹	H5, W4	5.528	11.63	24.6	0.16	2.12
Kerman 002 ¹	L6, W3	2.958	10.28	24.47	0.12	2.38
Kerman 003 ²	L5, W2	2.435	15.77	26.79	0.28	1.70
Lut 001 ¹	H5, W3	3.613	14.78	27.35	0.24	1.85
Lut 003 ¹	L3, W3	5.066	13.35	24.33	0.25	1.82

¹Ruzicka et al. (2017).

²Bouvier et al. (2017).

³Saturation magnetization.

⁴Coercivity.

⁵Coercivity of remanence.

⁶Saturation remanent magnetization.

XRD Data

The modal mineralogy deduced from XRD analysis of a selection of nine H, L, and LL heavily weathered (W3–W5) meteorites from different regions of the Lut Desert (Kerman and Lut DCAs) is reported in Table 5. Besides the usual primary minerals (olivine, pyroxene, anorthite, metal, troilite) found in OCs, the following weathering products were detected: hematite, maghemite, goethite, akaganéite, and magnetite. Figure S4 in supporting information shows the diffractograms of Kerman 003 and Lut 009 that represent the least and most oxidized meteorites analyzed in this work. The degree of weathering estimated by means of XRD phase analysis reveals that total oxidation (sum of the modal abundances of the weathering products) for the Lut Desert samples ranges from 11 to 27 wt% (equivalent to 42–78 atom% Fe). The comparison of the total oxide minerals abundance of the H and L chondrites from the Lut Desert does not show any correlation between the group and the weathering of the meteorites. As shown in Fig. 6, a positive correlation exists between the abundance of maghemite and total iron oxides. More weathered samples show higher maghemite contents. A comparison of our data for the Lut Desert meteorites with meteorites from the San Juan DCA in the Atacama Desert (Munayco et al. 2013) shows differences between their oxidation products (Fig. 6). The Lut Desert meteorites show higher iron oxides abundance than those from San Juan. This is in agreement with the much wetter present day and past climate (over the Holocene) in the Lut Desert compared to the Atacama Desert. Maghemite, goethite, and hematite are the dominant weathering phases in the Lut Desert meteorites, whereas goethite is the dominant phase in the San Juan samples and hematite is absent. The dominance of goethite in less-weathered San Juan

Table 5. Phase modal abundances of selected ordinary chondrites from the Lut Desert obtained by XRD analysis.

Meteorite	Type	Silicates			Opauques		Iron oxides				
		Olivine	Pyroxene	Anorthite	FeNi metal	Troilite	Goethite	Hematite	Maghemite	Magnetite	Akaganéite
Kerman 001 ¹	H5, W4	42.36	40.09	1.75	0.00	3.10	5.60	0.00	7.11	0.00	0.00
Kerman 002 ¹	L6, W3	49.5	33.75	3.26	0.00	0.94	1.61	2.61	8.33	0.00	0.00
Kerman 003 ²	L5, W2	47.64	33.58	6.1	0.00	1.93	5.07	2.19	3.49	0.00	0.00
Lut 001 ¹	H5, W3	37.79	37.82	7.11	0.00	1.31	7.27	0.00	8.71	0.00	0.00
Lut 003 ¹	L3, W3	35.11	32.35	6.59	0.00	1.14	8.25	1.66	14.91	0.00	0.00
Lut 006 ¹	LL3, W3	55.33	11.45	8.38	0.11	0.08	5.08	1.71	13.21	1.15	3.51
Lut 008 ¹	H4, W5	35.82	32.68	5.48	0.00	1.95	6.20	7.05	10.82	0.00	0.00
Lut 009 ²	H4, W4	41.17	21.34	10.04	0.00	0.26	8.35	0.51	18.33	0.00	0.00
Shahdad ³	H5, W4	37.42	29.86	8.62	0.00	2.48	8.58	1.63	11.41	0.00	0.00

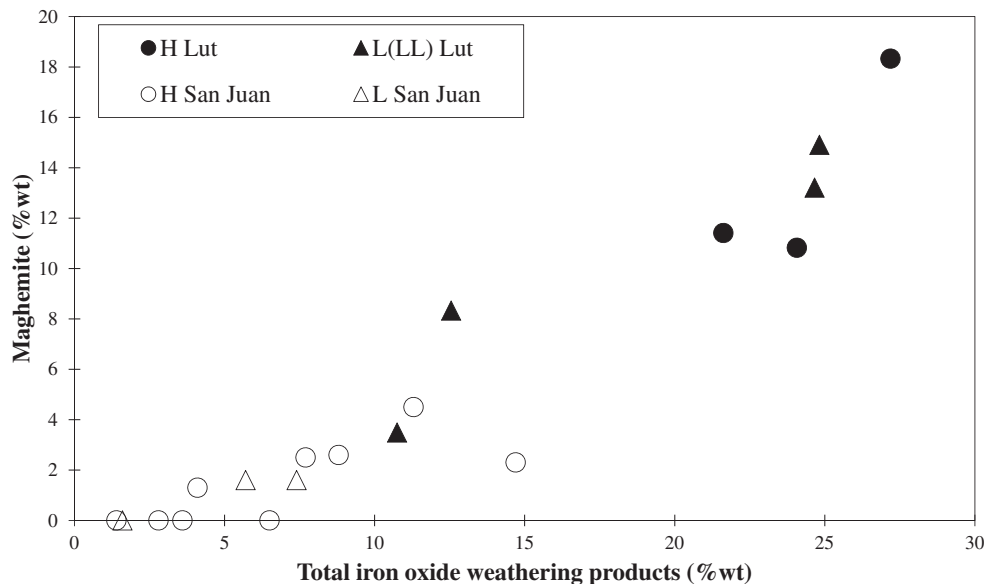
¹Ruzicka et al. (2017).²Bouvier et al. (2017a).³Gravie (2012).

Fig. 6. Total iron oxide weathering products (%) versus maghemite (%) contents in the Lut meteorites. Data obtained by XRD. San Juan data from Munayco et al. (2013).

samples might be considered as a lower level of oxidation, which is later followed by its transformation to hematite and later to maghemite (e.g., Stanjek 1987).

Geochemistry

Major and Trace Element Composition

The whole rock major, minor, and trace element chemical composition of nine H, L, and LL heavily weathered (W3–W5) meteorites from different regions of the Lut Desert (Kerman and Lut DCAs) along with two samples from the Atacama Desert (EM 049 and CeC 006) and one sample from Sahara Desert (Aridal

006) are reported in Table 6. The last three meteorites from other deserts were chosen because of their high weathering degrees (see Pourkhorsandi et al. 2017b). Chemical modification of these meteorites compared to the average composition of their corresponding chondrite groups and in relation to the bulk soil composition is shown in Fig. 7.

Desert weathering has changed the chemical composition of the meteorites. In relation to the bulk soil composition (given in Table S1), elements with higher abundance in the soil and relatively mobile behavior like Th, U, Mo, Sr, Ba, Li, Pb, and Tl are enriched in the meteorites. The higher contents of these

Table 6. *Continued.* Whole rock major, minor, and trace element chemical composition of selected Lut Desert OCs along with two from Atacama (EM 049 and CeC 006) and one sample from the Sahara Desert (Aridal 006) and Kilabo fall. Major elements data were obtained by ICP-OES and minor and trace elements were measured using ICP-MS.

	Kerman			Lut			Lut 008 ¹	Lut 009 ²	Shahdad ³	Aridal 006 ²	CeC 006 ⁴	EM 049 ⁵	Kilabo ⁶
	001 ¹	002 ¹	003 ²	Lut 001 ¹	Lut 003 ¹	Lut 006 ¹							
Ho ⁷ ($\mu\text{g g}^{-1}$)	0.08	0.08	0.08	0.06	0.07	0.08	0.07	0.07	0.07	0.06	0.10	0.10	n.d.
Er ⁷ ($\mu\text{g g}^{-1}$)	0.22	0.24	0.24	0.20	0.20	0.24	0.20	0.20	0.20	0.18	0.31	0.30	n.d.
Tm ⁷ ($\mu\text{g g}^{-1}$)	0.03	0.03	0.03	0.03	0.03	0.04	0.03	0.03	0.03	0.03	0.04	0.04	n.d.
Yb ⁷ ($\mu\text{g g}^{-1}$)	0.22	0.23	0.24	0.20	0.19	0.26	0.20	0.20	0.21	0.18	0.28	0.27	n.d.
Lu ⁷ ($\mu\text{g g}^{-1}$)	0.03	0.04	0.04	0.03	0.03	0.03	0.03	0.03	0.03	0.03	0.04	0.04	n.d.
Hf ($\mu\text{g g}^{-1}$)	0.16	0.15	0.15	0.16	0.14	0.22	0.13	0.14	0.15	0.16	0.16	0.16	n.d.
W ($\mu\text{g g}^{-1}$)	0.07	0.13	0.19	0.06	0.49	0.02	0.29	0.22	0.16	0.07	0.81	0.19	n.d.
Tl ($\mu\text{g g}^{-1}$)	0.37	<0.01	<0.01	0.14	0.18	0.17	0.03	0.14	0.29	<0.01	0.27	0.13	n.d.
Pb ($\mu\text{g g}^{-1}$)	0.57	1.08	0.27	0.30	0.55	0.37	0.36	0.36	0.55	0.17	0.43	0.33	n.d.
Th ($\mu\text{g g}^{-1}$)	0.07	0.07	0.09	0.22	0.07	0.15	0.06	0.10	0.21	0.09	0.19	0.15	n.d.
U ($\mu\text{g g}^{-1}$)	0.10	0.07	0.06	0.07	0.09	0.38	0.04	0.28	0.18	0.04	0.27	0.10	n.d.
Ta ($\mu\text{g g}^{-1}$)	0.02	0.03	0.02	0.03	0.02	0.03	0.02	0.03	0.03	0.03	0.03	0.03	n.d.

n.d. = not determined.

¹Ruzicka et al. (2017).

²Bouvier et al. (2017a).

³Garvie (2012).

⁴Ruzicka et al. (2014).

⁵Ruzicka et al. (2015).

⁶Russell et al. (2003).

⁷Pourkhorsandi et al. (2017b).

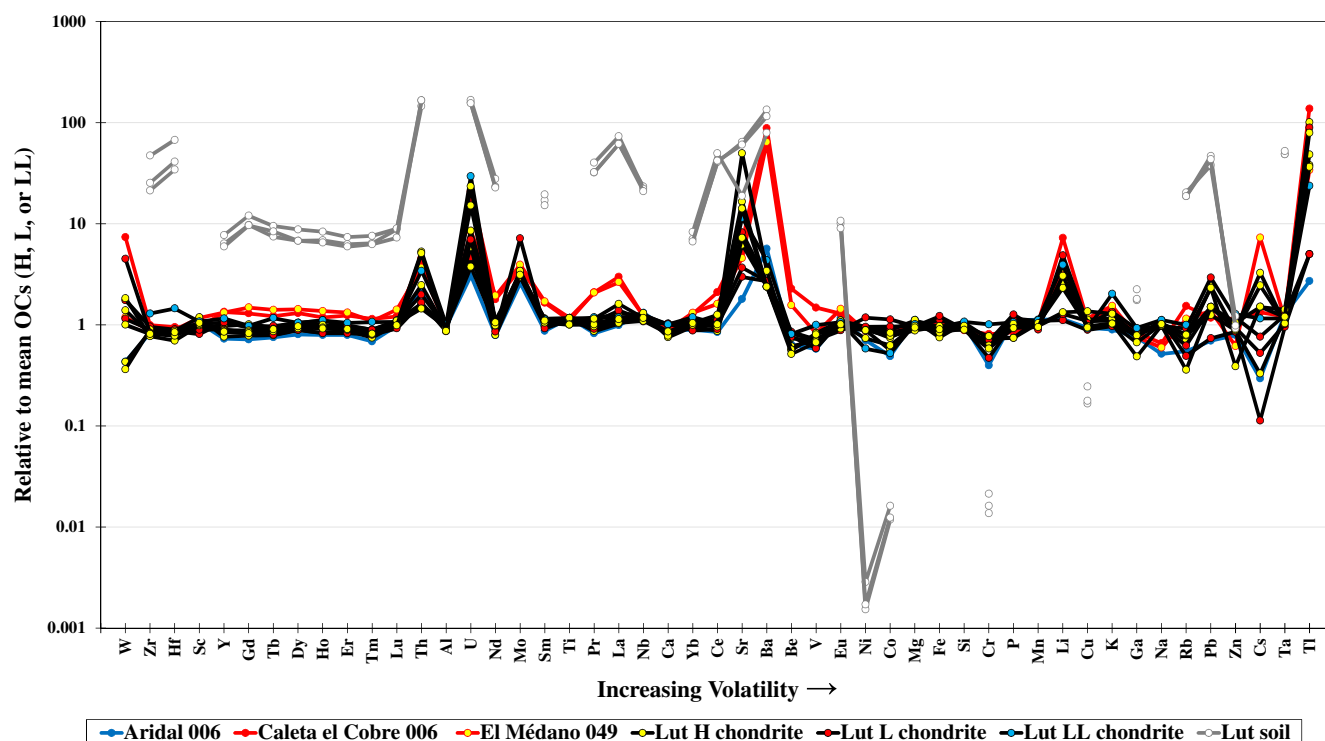


Fig. 7. Normalized spider diagrams of bulk compositions of OCs from the Lut, Atacama, and Sahara deserts. Each chondrite is normalized to the mean composition of its corresponding group (mean composition data from Wasson and Kallemeyn 1988). Strontium, Ba, and the REE composition data source: Pourkhorsandi et al. (2017b). Soil composition data shown for comparison, are normalized to average OCs composition (data source: McDonough and Sun 1995). (Color figure can be viewed at wileyonlinelibrary.com.)

elements in hot desert meteorites is reported by various workers (Stelzner et al. 1999; Al-Kathiri et al. 2005; Folco et al. 2007; Hezel et al. 2011; Pourkhorsandi et al. 2017b). A decrease in the contents of V, Cr, Co, Rb due to desert weathering is detectable. In addition, Fe shows a possible depletion in the H chondrites. Some elements, such as Cs and W, show variable behavior. Possibly different contents of these elements in the underlying soil might be a reason for this observation. As observed in meteorites from other hot deserts (e.g., Hezel et al. 2011), major element contents are stable during desert weathering process.

In comparison to Lut Desert meteorites, CeC 006 and EM 049 are showing similar anomaly patterns. However, as reported by Pourkhorsandi et al. (2017b) and shown in Fig. 7, as a consequence of different weathering regimes, the abundances of elements such as REEs (in particular LREE), Sr, and Ba in meteorites from different deserts is contrasted.

LOI Contents

Sequential LOI analysis is a common method to estimate the water content, organic matter, inorganic carbon, and mineralogenic residue in terrestrial rock and sediment samples. Heating to different temperatures

causes various phases to decompose, which is usually reflected as the weight deviation from the initial mass (Heiri et al. 2001; Santisteban et al. 2004).

In order to document the effects of terrestrial weathering on LOI contents of meteorites, we selected nine H, L, and LL heavily weathered (W3–W5) meteorites from different regions of the Lut Desert (Kerman and Lut DCAs). In addition, three previously mentioned finds from the Atacama and Sahara deserts and Kilabo LL6 fall were analyzed. All meteorites lost 0.8% of their weight after heating up to 110 °C (Table S2 in supporting information) (Fig. 8). This temperature marks the removal of free water (moisture) from the samples. Record of the released organic carbon and combined water from hydroxyl iron minerals can be achieved by heating the sample up to 550 °C. On average, hot desert meteorites lost 3.9% of their initial mass. The next step of heating (up to 850 °C) leads to the decomposition of any carbon-rich compound, secondary carbonates included, and at the same time oxidation of metal and troilite to hematite which causes the weight increase and the color change in the samples. A weight loss is observed for the majority of Lut samples (e.g., Shahdad), indicating the presence of carbonates, especially calcite. In contrast, the weight increase after this heating step for samples like Kilabo, EM 049, Kerman

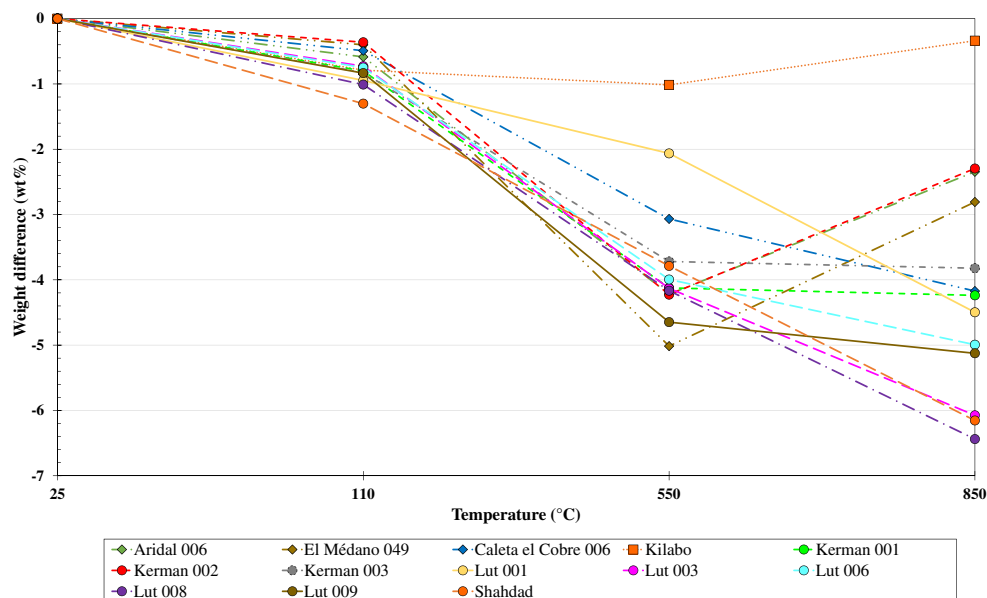


Fig. 8. Plotted data of sequential combustion showing mass differences as a function of heat. (Color figure can be viewed at wileyonlinelibrary.com.)

002, and Aridal 006 shows their very low concentrations of carbonates.

Carbon and Nitrogen Contents

The decrease in TC content of the OCs with increasing parent body thermal metamorphism has been evidenced in different works (e.g., Moore and Lewis 1967). Terrestrial weathering is another process known to be able to increase TC (Gibson and Bogard 1978; Ash and Pillinger 1993).

Sequential combustion and mass loss measurements on the same batch of meteorites as for previous analyses from the Lut Desert was conducted. Our data show that the Lut Desert meteorites have higher TC than falls (Fig. 9a; Table 7). Comparison of the TC, TOC, and CaCO_3 contents show that the Lut Desert samples are richer than those from the Atacama and Sahara deserts (Fig. 9b). TC shows a good correlation with the CaCO_3 content, which demonstrates that CaCO_3 is more responsible than TOC for the higher TC content of these meteorites. In other words, it rules out the idea of higher TC in the Lut Desert samples because of a possible higher concentration of indigenous carbon in the unweathered samples.

It is also noteworthy that the strongly weathered (W4) Shahdad meteorite shows the highest concentrations of these components as well as an abnormally high (0.104 wt%) nitrogen content. This might be related to the presence of terrestrial nitrate minerals. Except Shahdad, nitrogen abundances of the

other meteorite samples are in the range of the values reported for other OCs (Kung and Clayton 1978).

CONCLUSIONS

With over 200 meteorites collected and classified, our field work confirms the suitability of the Lut Desert, particularly Kalut, for the preservation and accumulation of meteorites. So far, all of the collected meteorites from the Lut Desert are OCs. The majority of the collected samples belong to two main strewnfields, of H5 and L5 classification, formed by two large meteorite showers located in Kalut, with dimensions being about 8×6 and 8×7 km, respectively. Most the H5 have a weathering degree of W3, while L5 are mostly W2. Considering a similar climatic conditions in the fall area, better preservation of the L5 meteorites compared to the H5 meteorites is suggesting a more recent age for the former. Assuming that all other finds outside of these two strewnfields are unpaired, the total number of unpaired meteorites found in Lut Desert would be about 36.

Terrestrial weathering is intense and has modified the geochemistry and mineralogy of the Lut Desert meteorites. Li, Sr, Mo, Ba, Tl, Th, and U are enriched in the analyzed samples. Meanwhile, V, Cr, Co, Rb (and possibly Fe) contents have decreased during meteorite weathering. Sequential combustion data show a higher abundance of carbonates (CaCO_3) in the Lut Desert OCs relative to Kilabo LL6 fall and EM 049

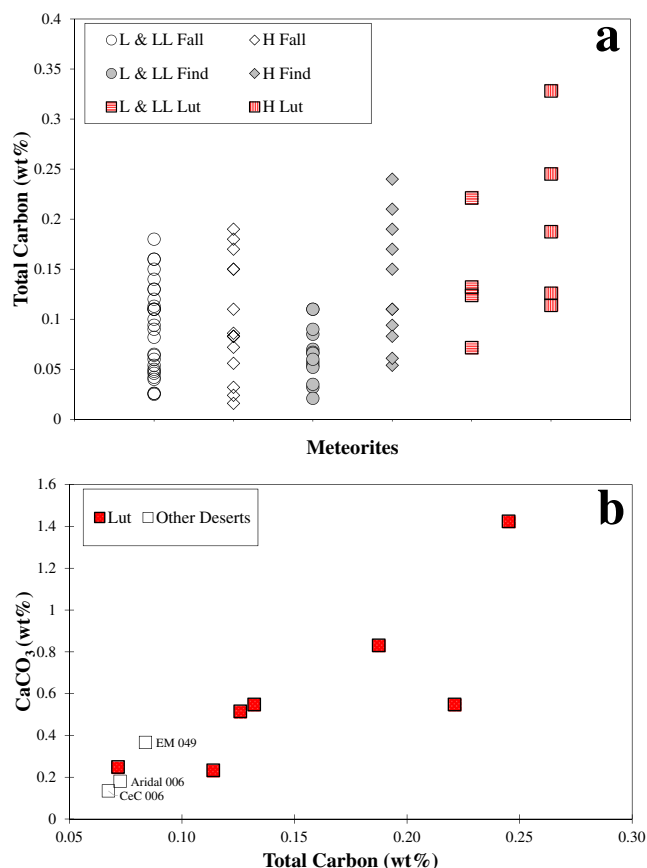


Fig. 9. a) Comparison of total carbon contents of find and fall petrologic type >3 OCs with the Lut Desert meteorites. Data source of the non-Lut samples: Moore and Lewis (1967). b) Total carbon versus carbonate content of the Lut desert OCs compared to three samples from the Atacama (CeC 006 and EM 049) and Sahara (Aridal 006) deserts. (Color figure can be viewed at wileyonlinelibrary.com.)

and Aridal 006 finds from the Atacama and Sahara deserts, respectively. This also applies for TC, TOC, and total abundance of iron oxyhydroxides, which are higher in these meteorites compared to the fall (for total and organic carbon) and find samples from other hot deserts. Our data show that CaCO₃ is more responsible than TOC for the higher TC contents of these meteorites. The mineralogy of the weathering products shows differences compared to meteorites from other hot deserts, with a dominance of maghemite, goethite, and hematite, and a common weathering of troilite to marcasite and pyrite instead of the direction oxidation to iron oxyhydroxides observed in other hot deserts.

The terrestrial ages of three meteorites suggest that the maximum preservation age in the Lut Desert is about 30 kyr, similar to that in other hot desert meteorites (except for the older Atacama desert).

Table 7. Total carbon (TC), total nitrogen (N), total organic carbon (TOC), and CaCO₃ contents of analyzed samples.

Meteorite	Type	N (wt%)	TC (wt%)	TOC (wt%)	CaCO ₃ (wt%)
Kerman 001 ¹	H5, W4	0.011	0.328	n.d.	n.d.
Kerman 002 ¹	L6, W3	0.002	0.072	0.042	0.249
Kerman 003 ²	L5, W2	0.003	0.132	0.066	0.548
Lut 001 ¹	H5, W3	b.d.l.	0.187	0.088	0.831
Lut 003 ¹	L3, W3	0.002	0.221	0.066	0.548
Lut 006 ¹	LL3, W3	0.003	0.124	n.d.	n.d.
Lut 008 ¹	H4, W5	b.d.l.	0.126	0.064	0.515
Lut 009 ²	H4, W4	0.009	0.114	0.086	0.233
Shahdad ³	H5, W4	0.104	0.245	0.074	1.424
Aridal 006 ²	H6, W4	0.006	0.073	0.051	0.181
CeC 006 ⁴	L6, W3	0.009	0.067	0.051	0.135
EM 049 ⁵	H4, W3	0.014	0.084	0.040	0.367

n.d. = not determined. b.d.l. = below detection limit.

¹Ruzicka et al. (2017).

²Bouvier et al. (2017a).

³Garvie (2012).

⁴Ruzicka et al. (2014).

⁵Ruzicka et al. (2015).

Our work, as an initial study, indicates the good potential of the Lut area for the preservation of meteorites.

SAFETY ADVICE

Drug smugglers are present in the Lut Desert. Beside this, the Iranian police have planted landmines in some regions of the desert to block smuggling ways. Therefore, any field trip in the region, especially for foreign groups, should be done after obtaining proper permissions and guidance from the corresponding authorities.

Acknowledgments—This work has been partly supported by Center for International Scientific Studies & Collaboration (CISSC) and a PHC Gundishapur. The first author thanks the French Embassy in Tehran for a PhD thesis grant. H. Pourkhorsandi thanks the ERC StG ISOyC for present funding. H. Pourkhorsandi, V. Debaille, P. Rochette, and J. Gattacceca thank PHC Tournesol France/Belgium. We thank all the meteorite hunters who provided their time to collect and provide the samples for this study. F. Demory, F. Rostek, H. Miche, and J. P. Lorand are thanked for their help during the analysis. A. Rubin is thanked for providing Shahdad and Lut 001 thin sections and fragments. H. Pourkhorsandi thanks J. Hassanzadeh for fruitful discussions and guidance and M. Zadsaleh for

providing the satellite images. Y. Quesnel is thanked for preparing Fig. 4b. We thank B. Devouard, K. Metzler, and M. Gounelle for their comments on earlier versions of this manuscript. We thank University of Tehran and Iranian National Institute for Oceanography and Atmospheric Science for their help during field and laboratory works. R. de Avillez thanks for the CNPq grant 305095/2015-3. V. Debaille thanks the FNRS-FRS and the ERC StG ISoSyC for present funding. We appreciate detailed and useful comments by the associate editor Dr. A. Ruzicka and reviewers Dr. M. Hutson and Dr. A. Hutzler.

Editorial Handling—Prof. Alexander Ruzicka

REFERENCES

- Adib D. and Liou J. G. 1979. The Naragh meteorite—A new olivine-bronzite chondrite fall. *Meteoritics* 14:257–272. <http://adsabs.harvard.edu/abs/1979Metic.14.257A>.
- Aghanabati A. 2004. *Geology of Iran*. Tehran, Iran: Geological Survey of Iran.
- Al-Kathiri A., Hofmann B. A., Jull A. J. T., and Gnos E. 2005. Weathering of meteorites from Oman: Correlation of chemical and mineralogical weathering proxies with ¹⁴C terrestrial ages and the influence of soil chemistry. *Meteoritics & Planetary Science* 40:1215–1239. <https://doi.org/10.1111/j.1945-5100.2005.tb00185.x/abstract>
- Ash R. D. and Pillinger C. T. 1993. Carbon in weathered ordinary chondrites from Roosevelt County. 24th Lunar and Planetary Science Conference. p. 43.
- Benedix G. K., Keil K., and Murakami J. Y. 1999. Classification of ten new Nullarbor Region meteorites. *Meteoritics & Planetary Science* 34:813–815.
- Bevan A. W. R. 1992. Australian meteorites. *Records of the Australian Museum Supplement* 15:1–27.
- Bevan A. W. R. and Binns R. A. 1989. Meteorites from the Nullarbor Region, Western Australia; I. A review of past recoveries and a procedure of naming new finds. *Meteoritics* 24:127–133.
- Bischoff A. 2001. Meteorite classification and the definition of new chondrite classes as a result of successful meteorite search in hot and cold deserts. *Planetary and Space Science* 49:769–776. <http://www.sciencedirect.com/science/article/pii/S0032063301000265>
- Bischoff A. and Geiger T. 1995. Meteorites from the Sahara: Find locations, shock classifications, degree of weathering and pairing. *Meteoritics & Planetary Science* 30:113–122. <https://doi.org/10.1111/j.1945-5100.1995.tb01219.x/abstract>
- Bland P. A., Berry F. J., Smith T. B., Skinner S. J., and Pillinger C. T. 1996. The flux of meteorites to the earth and weathering in hot desert ordinary chondrite finds. *Geochimica et Cosmochimica Acta* 60:2053–2059.
- Bland P. A., Sexton A. S., Jull A. J. T., Bevan A. W. R., Berry F. J., Thornley D. M., Astin T. R., Britt D. T., and Pillinger C. T. 1998. Climate and rock weathering: A study of terrestrial age dated ordinary chondritic meteorites from hot desert regions. *Geochimica et Cosmochimica Acta* 62:3169–3184. <http://www.sciencedirect.com/science/article/pii/S0016703798001999>
- Bland P. A., Zolensky M. E., Benedix G. K., and Sephton M. A. 2006. Weathering of chondritic meteorites. In *Meteorites and the early solar system II*, edited by Lauretta D. S. and McSween H. Y. Jr Tucson, Arizona: University of Arizona Press. pp. 853–867. <http://www.lpi.usra.edu/books/MESSII/9041.pdf>
- Bouvier A., Gattacceca J., Agee C., Grossman J., and Metzler K. 2017a. The Meteoritical Bulletin no. 104. *Meteoritics & Planetary Science* 52:2284. <https://doi.org/10.1111/maps.12930>
- Bouvier A., Gattacceca J., Grossman J., and Metzler K. 2017b. The Meteoritical Bulletin, no. 105. *Meteoritics & Planetary Science* 52:2411. <https://doi.org/10.1111/maps.12944>
- Clarke R. S. 1975. The Meteoritical Bulletin. *Meteoritics* 10:133–158. <https://doi.org/10.1111/j.1945-5100.1975.tb00018.x>
- Debaille V., Gattacceca J., Rochette P., Pourkhorsandi H., van Ginneken M., Leduc T., De Ceukelaire M., Goderis S., and Claeys P. 2017. Classification of Antarctic meteorites by magnetic susceptibility (abstract 42_01). *Proceedings of the Eighth Symposium on Polar Science*.
- Djamali M., Akhiani H., Khoshravesh R., Ponel P., and Brewer S. 2011. Application of the Global Bioclimatic Classification to Iran: implications for understanding the modern vegetation and biogeography. *Ecologia Mediterranea* 37:91–114.
- Dresch J. 1968. Reconnaissance dans le Lut (Iran). *Bulletin de l'Association de géographes français* 45:143–153.
- Ehsani A. H. and Quiel F. 2008. Application of self organizing map and SRTM data to characterize yardangs in the Lut desert, Iran. *Remote Sensing of Environment* 112:3284–3294.
- Ferrari M., Moggi-Cecchi V., Pratesi G., Di Martino M., Giuli G., Nemati M., and De Sanctis M. C. 2018. The second joint Italian–Iranian expedition to Dasht-e Lut for meteorite recovery. In *European Planetary Science Congress*. Berlin. p. 1030.
- Folco L., Rochette P., Gattacceca J., and Perchiazzi N. 2006. In situ identification, pairing, and classification of meteorites from Antarctica through magnetic susceptibility measurements. *Meteoritics & Planetary Science* 41:343–353. <https://doi.org/10.1111/j.1945-5100.2006.tb00467.x/abstract>
- Folco L., D’Orazio M., and Perchiazzi N. 2007. Authenticating the recovery location of meteorites: The case of Castenaso. *Meteoritics & Planetary Science* 42:321–330. <https://doi.org/10.1111/j.1945-5100.2007.tb00236.x>
- Garvie L. A. J. 2012. The Meteoritical Bulletin, no. 99. *Meteoritics & Planetary Science* 47:E1–E52. <https://doi.org/10.1111/maps.12026>
- Gattacceca J., Valenzuela M., Uehara M., Jull A. J. T., Giscarda M., Rochette P., Braucher R., Suavet C., Gounelle M., Morata D., Munayco P., Bourrot-Denis N., Bourles D., and Demory F. 2011. The densest meteorite collection area in hot deserts: The San Juan meteorite field (Atacama Desert, Chile). *Meteoritics & Planetary Science* 46:1276–1287. <https://doi.org/10.1111/j.1945-5100.2011.01229.x/full>
- Gattacceca J., Suavet C., Rochette P., Weiss B. P., Winkhofer M., Uehara M., and Friedrich J. M. 2014. Metal phases in ordinary chondrites: Magnetic hysteresis properties and implications for thermal history. *Meteoritics & Planetary Science* 49:652–676. <https://doi.org/10.1111/maps.12268>

- Gattacceca J., Bouvier A., Grossman J., Metzler K., and Uehara M. 2018. The Meteoritical Bulletin, No. 106. *Meteoritics & Planetary Science* 54:469–471. <https://doi.org/10.1111/maps.13215>
- Gattacceca J., Bouvier A., Grossman J., Metzler K., and Uehara M. 2019. The Meteoritical Bulletin, no. 107. *Meteoritics & Planetary Science*.
- Ghods M. 2017. Morphometric characteristics of Yardangs in the Lut Desert, Iran. *Desert* 22:21–29.
- Gibson E. K. J. and Bogard D. D. 1978. Chemical alterations of the Holbrook chondrite resulting from terrestrial weathering. *Meteoritics* 13:277–289.
- Gnos E., Lorenzetti S., Eugster O., Jull A. J. T., Hofmann B. A., Al-Khatiri A., and Eggimann M. 2009. The Jiddat al Harasis 073 strewn field, Sultanate of Oman. *Meteoritics & Planetary Science* 44:375–387. <https://doi.org/10.1111/j.1945-5100.2009.tb00739.x>
- Graham A. L. and Hassanzadeh J. 1990. The Meteoritical Bulletin. *Meteoritics* 25:59–63. <https://doi.org/10.1111/j.1945-5100.1990.tb00971.x>
- Harvey R. 2003. The origin and significance of Antarctic meteorites. *Chemie der Erde—Geochemistry* 63:93–147.
- Heiri O., Lotter A. F., and Lemcke G. 2001. Loss on ignition as a method for estimating organic and carbonate content in sediments: Reproducibility and comparability of results. *Journal of Paleolimnology* 25:101–110. <https://doi.org/10.1023/a:1008119611481>
- Hezel D. C., Schlüter J., Kallweit H., Jull A. J. T., Al Fakeer O. Y., Al Shamsi M., and Strekopytov S. 2011. Meteorites from the United Arab Emirates: Description, weathering, and terrestrial ages. *Meteoritics & Planetary Science* 46:327–336. <https://doi.org/10.1111/j.1945-5100.2010.01165.x/abstract>
- Hofmann B. A., Gnos E., Jull A. J. T., Szidat S., Majoub A., Al Wagdani K., Habibullah S. N., Halawani M., Hakeem M., Al Shanti M., and Al Somali A. 2018. Meteorite reconnaissance in Saudi Arabia. *Meteoritics & Planetary Science* 53:2372–2394. <https://doi.org/10.1111/maps.13132>
- Hutson M., Ruzicka A., Jull A. J. T., Smaller J. E., and Brown R. 2013. Stones from Mohave County, Arizona: Multiple falls in the “Franconia strewn field.” *Meteoritics & Planetary Science* 48:365–389. <https://doi.org/10.1111/maps.12062>
- Hutson M. L., Ruzicka A. M., and Nazari M. 2014. Diverse and unusual O-chondrites from the Lut Desert, Iran. *77th Annual Meeting of the Meteoritical Society*. p. A5180.
- Hutzler A., Gattacceca J., Rochette P., Braucher R., Carro B., Christensen E. J., Cournede C., Gounelle M., and Laridhi Ouazaa N. 2016. Description of a very dense meteorite collection area in western Atacama: Insight into the long-term composition of the meteorite flux to Earth. *Meteoritics & Planetary Science* 51:468–482. <https://doi.org/10.1111/maps.12607>
- Hyde B. C., Day J. M. D., Tait K. T., Ash R. D., Holdsworth D. W., and Moser D. E. 2014. Characterization of weathering and heterogeneous mineral phase distribution in brachinite Northwest Africa 4872. *Meteoritics & Planetary Science* 49:1141–1156. <https://doi.org/10.1111/maps.12320>
- Jull A. J. T., Donahue D. J., Cielaszyk E., and Wlotzka F. 1993. Carbon-14 terrestrial ages and weathering of 27 meteorites from the southern high plains and adjacent areas (USA). *Meteoritics* 28:188–195. <https://doi.org/10.1111/j.1945-5100.1993.tb00756.x>
- Jull A. J. T., Mchargue L. R., Bland P. A., Greenwood R. C., Bevan A. W. R., Kim K. J., Lamotta S. E., and Johnson J. A. 2010. Terrestrial ages of meteorites from the Nullarbor region, Australia, based on ^{14}C and ^{14}C - ^{10}Be measurements. *Meteoritics & Planetary Science* 45:1271–1283. <https://doi.org/10.1111/j.1945-5100.2010.01289.x/full>
- Kent J. J., Brandon A. D., Joy K. H., Peslier A. H., Lapen T. J., Irving A. J., and Coleff D. M. 2017. Mineralogy and petrogenesis of lunar magnesian granulitic meteorite Northwest Africa 5744. *Meteoritics & Planetary Science* 52:1916–1940. <https://doi.org/10.1111/maps.12898>
- Kring D., Jull A., McHargue L., Bland P., Hill D., and Berry F. 2001. Gold basin meteorite strewn field, Mojave Desert, northwestern Arizona: Relic of a small late Pleistocene impact event. *Meteoritics & Planetary Science* 36:1057–1066. <http://oro.open.ac.uk/5771/>
- Kung C.-C. and Clayton R. N. 1978. Nitrogen abundances and isotopic compositions in stony meteorites. *Earth and Planetary Science Letters* 38:421–435. <http://linkinghub.elsevier.com/retrieve/pii/0012821X78901176>
- Lee M. R. and Bland P. A. 2003. Dating climatic change in hot deserts using desert varnish on meteorite finds. *Earth and Planetary Science Letters* 206:187–198.
- Li S., Wang S., Leya I., Smith T., Tang J., Wang P., Zeng X. I., and Li Y. 2017. A chondrite strewn field was found in east of Lop Nor, Xinjiang. *Chinese Science Bulletin* 62:2407–2415.
- Mashhadi N., Alavipanah S. K., and Ahmadi H. 2002. Geomorphology studies of Lout yardangs. *Desert (Biaban)* 7:25–43.
- McDonough W. F. and Sun S. S. 1995. The composition of the Earth. *Chemical Geology* 120:223–253. <http://linkinghub.elsevier.com/retrieve/pii/0009254194001404>
- Merriam D. F. and Harbaugh J. W. 2007. Meteorites and possible meteorite impact features in Kansas. *Transactions of the Kansas Academy of Science* 110:61–69.
- Mildrexler D. J., Zhao M., and Running S. W. 2006. Where are the hottest spots on Earth? *Eos, Transactions American Geophysical Union* 87:461–467. <https://doi.org/10.1029/2006eo430002>
- Mildrexler D. J., Zhao M., and Running S. W. 2011. Satellite finds highest land skin temperatures on Earth. *Bulletin of the American Meteorological Society* 92:855–860. journals.ametsoc.org/doi/pdf/10.1175/2011bams3067.1
- Moggi-Cecchi V., Cecchi L., Pratesi G., Giuli G., Nemati M., Di Martino M., and Serra R. 2017. Preliminary results of the Lut Desert 2017 Joint Italian-Iranian Expedition for Meteorite Recovery. 80th Annual Meeting of the Meteoritical Society. (abstract #6306). *Meteoritics & Planetary Science* 52.
- Moore C. B. and Lewis C. F. 1967. Total carbon content of ordinary chondrites. *Journal of Geophysical Research* 72:6289.
- Motamed A. 1974. Geography and climate of Lut Iran. *Geographical Research Quarterly* 11:3–13. <http://www.noormags.ir/view/en/articlepage/336794/>
- Munayco P., Munayco J., de Avillez R. R., Valenzuela M., Rochette P., Gattacceca J., and Scorzelli R. B. 2013. Weathering of ordinary chondrites from the Atacama Desert, Chile, by Mössbauer spectroscopy and synchrotron radiation X-ray diffraction. *Meteoritics & Planetary Science* 48:457–473. <https://doi.org/10.1111/maps.12067>

- Muñoz C., Guerra N., Martínez-Frías J., Lunar R., and Cerda J. 2007. The Atacama Desert: A preferential arid region for the recovery of meteorites—Find location features and strewfield distribution patterns. *Journal of Arid Environments* 71:188–200.
- Ouazaa N. L., Perchiazzi N., Kassaa S., Ghanmi M., and Folco L. 2009. Meteorite finds from southern Tunisia. *Meteoritics & Planetary Science* 44:955–960.
- Pailler D. and Bard E. 2002. High frequency palaeoceanographic changes during the past 140,000 yr recorded by the organic matter in sediments of the Iberian Margin. *Palaogeography, Palaeoclimatology, Palaeoecology* 181:431–452. <http://linkinghub.elsevier.com/retrieve/pii/S0031018201004448>
- Pastukhovich A. Y., Larionov M. Y., Kruglikov N. A., Zamyatin D. A., and Grokhovsky V. I. 2017. URFU meteorite expedition to the Lut Desert (Iran). 80th Annual Meeting of the Meteoritical Society. p. 6356.
- Pourkhorsandi H. and Mirnejad H. 2013. Lut Desert (Iran): A high-potential area for finding meteorites (abstract #1096). 44th Lunar and Planetary Science Conference. CD-ROM.
- Pourkhorsandi H., Gattacceca J., Devouard B., D’Orazio M., Rochette P., Beck P., Sonzogni C., and Valenzuela M. 2017a. The ungrouped chondrite El Médano 301 and its comparison with other reduced ordinary chondrites. *Geochimica et Cosmochimica Acta* 218:98–113. <http://linkinghub.elsevier.com/retrieve/pii/S0016703717305689>
- Pourkhorsandi H., D’Orazio M., Rochette P., Valenzuela M., Gattacceca J., Mirnejad H., Sutter B., Hutzler A., and Aboulahris M. 2017b. Modification of REE distribution of ordinary chondrites from Atacama (Chile) and Lut (Iran) hot deserts: Insights into the chemical weathering of meteorites. *Meteoritics & Planetary Science* 52:1843–1858. <https://doi.org/10.1111/maps.12894>
- Rochette P., Sagnotti L., Bourot-Denise M., Consolmagno G., Folco L., Gattacceca J., Osete M. L., and Pesonen L. 2003. Magnetic classification of stony meteorites: 1 Ordinary chondrites. *Meteoritics & Planetary Science* 38:251–268. <https://doi.org/10.1111/j.1945-5100.2003.tb00263.x>
- Rochette P., Gattacceca Bonal L., Bourot-Denis M., Chevrier V., Clerc J. P., Consolmagno G., Folco L., Gounelle M., Kohout T., Pesonen L., Quirico E., Sagnotti L., and Skripnik A. 2008. Magnetic classification of stony meteorites: 2. Non-ordinary chondrites. *Meteoritics & Planetary Science* 43:959–980. <https://doi.org/10.1111/j.1945-5100.2008.tb01092.x>
- Rochette P., Gattacceca J., Bourot-Denise M., Consolmagno G., Folco L., Kohout T., Pesonen L., and Sagnotti L. 2009. Magnetic classification of stony meteorites: 3. Achondrites. *Meteoritics & Planetary Science* 44:405–427. <https://doi.org/10.1111/j.1945-5100.2009.tb00741.x>
- Rochette P., Gattacceca J., and Lewandowski M. 2012. Magnetic classification of meteorites and application to the Softman fall. *Meteorites* 2:67–71. <https://doi.org/10.5277/met120108>.
- Rubin A. E. and Read W. F. 1984. The Brownell and Ness County (1894) L6 chondrites: further sorting-out of Ness County meteorites. *Meteoritics* 19:153–160. <https://doi.org/10.1111/j.1945-5100.1984.tb00038.x>
- Rubin A. E., Verish R. S., Moore C. B., and Oriti R. A. 2000. Numerous unpaired meteorites exposed on a deflating playa lake at Lucerne Valley, California. *Meteoritics & Planetary Science* 35:A181–A183. <https://doi.org/10.1111/j.1945-5100.2000.tb01793.x>
- Russell S. S., Zipfeel J., Folco L., Jones R., Grady M. M., McCoy T., and Grossman J. N. 2003. The Meteoritical Bulletin, No. 87, 2003 July. *Meteoritics & Planetary Science* 38:A189–A248. <https://doi.org/10.1111/j.1945-5100.2003.tb00328.x>.
- Ruzicka A., Grossman J. N., and Garvie L. 2014. The Meteoritical Bulletin, No. 100, 2014 June. *Meteoritics & Planetary Science* 49:E1–E101. <https://doi.org/10.1111/maps.12342>
- Ruzicka A., Grossman J., Bouvier A., Herd C. D. K., and Agee C. B. 2015. The Meteoritical Bulletin, no. 101. *Meteoritics & Planetary Science* 50:1661. <https://doi.org/10.1111/maps.12490>
- Ruzicka A., Grossman J., Bouvier A., and Agee C. B. 2017. The Meteoritical Bulletin, no. 103. *Meteoritics & Planetary Science* 52:1014. <https://doi.org/10.1111/maps.12888>
- Santisteban J. I., Mediavilla R., López-Pamo E., Dabrio C. J., Ruiz Zapata M. B., Gil García M. J., Castaño S., and Martínez-Alfaro P. E. 2004. Loss on ignition: A qualitative or quantitative method for organic matter and carbonate mineral content in sediments? *Journal of Paleolimnology* 32:287–299. <https://doi.org/10.1023/b:jopl.0000042999.30131.5b>
- Saunier G., Poitrasson F., Moine B., Gregoire M., and Seddiki A. 2010. Effect of hot desert weathering on the bulk-rock iron isotope composition of L6 and H5 ordinary chondrites. *Meteoritics & Planetary Science* 45:195–209. <https://doi.org/10.1111/j.1945-5100.2010.01017.x/full>
- Schlüter J., Schultz L., Thiedig F., Al-Mahdi B. O., and Abu Aghreb A. E. 2002. The Dar al Gani meteorite field (Libyan Sahara): Geological setting, pairing of meteorites, and recovery density. *Meteoritics* 37:1079–1093.
- Schoonen M. A. A. and Barnes H. L. 1991. Reactions forming pyrite and marcasite from solution: II. Via FeS precursors below 100°C. *Geochimica et Cosmochimica Acta* 55:1505–1514.
- Smith D. L., Ernst R. E., Samson C., and Herd R. 2006. Stony meteorite characterization by non-destructive measurement of magnetic properties. *Meteoritics & Planetary Science* 41:355–373. <https://doi.org/10.1111/j.1945-5100.2006.tb00468.x>
- Soulet G., Ménot G., Garreta V., Rostek F., Zaragosi S., Lericolais G., and Bard E. 2011. Black Sea “Lake” reservoir age evolution since the Last Glacial — Hydrologic and climatic implications. *Earth and Planetary Science Letters* 308:245–258. <http://linkinghub.elsevier.com/retrieve/pii/S0012821X11003505>
- Stanjek H. 1987. The formation of maghemite and hematite from lepidocrocite and goethite in a Cambisol from Corsica, France. *Zeitschrift für Pflanzenernährung und Bodenkunde* 150:314–318. <https://doi.org/10.1002/jpln.19871500509>
- Stelzner T., Heide K., Bischoff A., Weber D., Scherer P., Schlutz L., Happel M., Schron W., Neupert U., Michel R., Clayton R. N., Mayeda T. K., Bonani G., Haidas I., Ivy-Ochs S., and Suter M. 1999. An interdisciplinary study of weathering effects in ordinary chondrites from the Acfer region, Algeria. *Meteoritics & Planetary Science* 34:787–794.
- Stocklin J. 1968. Structural history and tectonics of Iran: A review. *AAPG Bulletin* 52:1229–1258. <https://doi.org/10.1306/5d25c4a5-16c1-11d7-8645000102c1865d>

- Uehara M., Gattacceca J., Rochette P., Demory F., and Valenzuela E. M. 2012. Magnetic study of meteorites recovered in the Atacama desert (Chile): Implications for meteorite paleomagnetism and the stability of hot desert surfaces. *Physics of the Earth and Planetary Interiors* 200–201:113–123. <https://doi.org/10.1016/j.pepi.2012.04.007>
- Van Schmus W. R. and Wood J. A. 1967. A chemical-petrologic classification for the chondritic meteorites. *Geochimica et Cosmochimica Acta* 31:747–765. <http://www.sciencedirect.com/science/article/pii/S0016703767800309> (accessed July 1, 2015).
- Ward H. A. 1901. Veramin meteorite. *American Journal of Science*. s4–12: 453–459. <https://doi.org/10.2475/ajs.s4-12.72.453>
- Wasson J. T. and Kallemeyn G. W. 1988. Compositions of chondrites. *Philosophical Transactions of the Royal Society A: Mathematical, Physical and Engineering Sciences* 325:535–544. <https://doi.org/10.1098/rsta.1988.0066>
- Welten K. C., Nishiizumi K., Finkel R. C., Hillegonds D. J., Jull A. J. T., Franke L., and Schultz L. 2004. Exposure history and terrestrial ages of ordinary chondrites from the Dar al Gani region, Libya. *Meteoritics & Planetary Science* 39:481–498. <https://doi.org/10.1111/j.1945-5100.2004.tb00106.x>
- Wlotzka F. 1993. A weathering scale for the ordinary chondrites. *Meteoritics* 28:460.
- Yousefi S. J., Moradian A., and Ahmadipour H. 2017. Petrogenesis of Plio-Quaternary basanites in the Gandom Beryan area, Kerman, Iran: Geochemical evidence for the low-degree partial melting of enriched mantle. *Turkish Journal of Earth Sciences* 26:284–301. <http://online.journals.tubitak.gov.tr/openDoiPdf.htm?mKodu=yer-1610-22>
- Zeng X., Li S., Leya I., Wang S., Smith T., Li Y., and Wang P. 2018. The Kumtag 016 L5 strewn field, Xinjiang Province, China. *Meteoritics & Planetary Science* 53:1113–1130. <https://doi.org/10.1111/maps.13073>
- Zolensky M. E., Wells G. L., and Rendell H. M. 1990. The accumulation rate of meteorite falls at the earth's surface—The view from Roosevelt County, New Mexico. *Meteoritics* 25:11–17.
- Zurfluh F. J., Hofmann B. A., Gnos E., and Eggenberger U. 2013. “Sweating meteorites”—Water-soluble salts and temperature variation in ordinary chondrites and soil from the hot desert of Oman. *Meteoritics & Planetary Science* 48:1958–1980. <https://doi.org/10.1111/maps.12211/abstract>
- Zurfluh F. J., Hofmann B. A., Gnos E., Eggenberger U., and Jull A. J. T. 2016. Weathering of ordinary chondrites from Oman: Correlation of weathering parameters with 14 C terrestrial ages and a refined weathering scale. *Meteoritics & Planetary Science* 51:1685–1700. <https://doi.org/10.1111/maps.12690>

SUPPORTING INFORMATION

Additional supporting information may be found in the online version of this article:

Table S1. Trace element chemical composition of three soil samples (KS1-3) and two reference materials (BHVO-1 and BHVO-2) analyzed by ICP-MS.

Table S2. The data of the mass loss during sequential combustion.

Figure S1. Topographic map of the Lut Desert.

Figure S2. Aerial photo of the Kalut. Image credit: George Steinmetz (georgesteinmetz.com).

Figure S3. Hysteresis loops obtained for the analyzed meteorites.

Figure S4. XRD pattern for (a) Kerman 003 and (b) Lut 009 meteorite. XRD data shows that Lut 009 is the most oxidized sample of this work, while Kerman 003 presents the lowest amount of iron oxides.